Available online at www.sciencedirect.com

ScienceDirect

Current Opinion in Chemical Engineering

Diffusing uphill with James Clerk Maxwell and Josef Stefan

Rajamani Krishna

The primary objective of this article is to highlight a number of situations of importance in chemical engineering in which one of the components in a mixture is transported uphill of its own composition gradient. The proper appreciation and modeling of uphill diffusion requires the use of chemical potential gradients as driving forces. Furthermore, due account needs to be taken of coupling effects, that is, the influence of the driving force of any component in the mixture on the transport fluxes of all partner species in the mixture. The Maxwell–Stefan formulation, that has its roots in theory of irreversible thermodynamics, affords the most general, and convenient, approach for modeling diffusion in fluid mixtures, electrolytes, alloys, glasses, and porous adsorbents.

Address
Van 't Hoff Institute for Molecular Sciences, University of Amsterdam, Science Park 904, 1098 XH Amsterdam, The Netherlands

Corresponding author: Krishna, Rajamani (r.krishna@contact.uva.nl)

Current Opinion in Chemical Engineering 2016, **12**:106–119

This review comes from a themed issue on **Separation engineering**

Edited by **WS Winston Ho** and **K Li**

http://dx.doi.org/10.1016/j.coche.2016.04.003

Introduction

Fick's law, that relates the diffusion flux to the composition gradient,

$$J_i = -c_t D_i \left(\frac{dx_i}{dz}\right) \quad (1)$$

is widely used in chemical engineering practice for the design of separation equipment [1•,2•,3]. The Fick diffusivity is usually positive definite, that is, $D_i > 0$, and the flux of species i is directed down its composition gradient. However, there are a number of examples for which Eq. (1) fails, even at a qualitative level, to describe the diffusion phenomena. Lars Onsager was amongst the first to recognize the limitations of Fick's law. In his classic paper published in 1945 entitled *Theories and Problems of Liquid Diffusion*, Onsager [4] wrote *The theory of liquid diffusion is relatively undeveloped... It is a striking symptom of the common ignorance in this field that not one of the phenomenological schemes which are fit to describe the general case of diffusion is widely known*. In the Onsager formalism for n-component mixture diffusion, the diffusion fluxes J_i are postulated to be linearly dependent on the chemical potential gradients, $d\mu_i/dz$, of each of the species present in the mixture.

A persuasive demonstration of the need to use $d\mu_i/dz$ as driving force, is available in the classic experiments reported in 1949 by Darken [5•]. In one of Darken's experiments, two austenite bars of different compositions (0.48% C, 3.8% Si, 95.72% Fe), and (0.45% C, 0.05% Si, 99.50% Fe) are welded together and maintained at 1323 K for a period of 13 days. The bars are then quenched and the C composition profiles determined; the results are shown in Figure 1. We note that C has diffused from the left-hand bar (with high Si content) to the right-hand bar (with low Si content). The high C content near the surface of the austenite bar on the right, imparts the required 'hardness' to steel. The process of hardening of steel by 'carburizing' is reliant on uphill transport of carbon from the high-Si bar to the low-Si bar, despite the fact that the initial compositions of carbon are practically the same in the two adjoining bars. In Table 3 of Darken's paper, the activity of carbon, defined by $a_1 = \gamma_1 x_1$, is calculated for the compositions A (0.315% C), and B (0.586% C); see Figure 1. The activity at A, $a_{1A} = 0.3$, while the activity at B, $a_{1B} = 0.29$. This implies that carbon diffuses down its activity gradient. In other words, the thermodynamic non-ideality effects are the root cause of uphill diffusion. Three quotes from the Darken paper [5•], summarize the foregoing arguments and serve as tramlines for the ensuing discussions and analysis:

"*the driving force in an isothermal diffusion process may be regarded as the gradient of the chemical potential*,",

"*for a system with more than two components it is no longer necessarily true that a given element tends to diffuse toward a region of lower concentration even within a single phase region*", and

"*departure from the behavior of an ideal solution may be so great that the concentration gradient and the chemical potential gradient, or activity gradient, may be of different sign, thus giving rise to uphill diffusion*".

The primary objective of this article is to highlight the importance of uphill transport in a wide variety of systems and scenarios that are of practical importance in the chemical, petrochemical and related industries. The first task is set up a convenient framework for describing multicomponent diffusion that can be applied for the solution of practical problems.

Figure 1

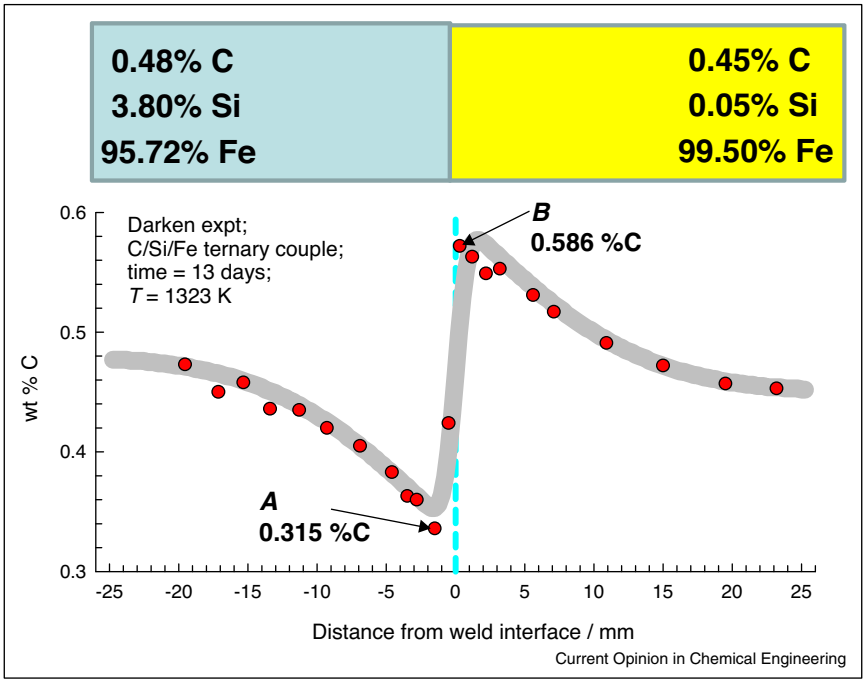

Experimental data of Darken [5•] for inter-diffusion between the left and right austenite bars consisting of C/Si/Fe mixtures. The wt% of each component is measured on either side of the Matano plane, measured at $t = 13$ days after the start of the experiment are shown.

The Maxwell–Stefan diffusion formulation

The approach we adopt stems from the pioneering works of James Clerk Maxwell [6] and Josef Stefan [7••], who analyzed diffusion in ideal gas mixtures. The Maxwell–Stefan (M–S) formulation is essentially a ''friction formulation'' in which the force acting on species i is balanced by friction with each of the partner species in the mixture [8••,9••] (a more detailed derivation is provided in the Supplementary material accompanying this publication):

$$-\frac{1}{RT}\frac{d\mu_i}{dz} = \sum_{j=1_{j\neq i}}^{n} \frac{x_j(u_i - u_j)}{Đ_{ij}}; \quad i = 1, 2, \ldots n \tag{2}$$

The pair diffusivity $Đ_{ij}$ can be interpreted as an inverse ''drag coefficient'' between species i and species j. Eq. (2) is consistent with the theory of irreversible thermodynamics; the Onsager reciprocal relations demand the symmetry constraint $Đ_{ij} = Đ_{ji}$. We define the fluxes $J_i \equiv c_t(u_i - u)$ with respect to the molar average mixture velocity, $u = x_1u_1 + x_2u_2 + \cdots x_nu_n$; in terms of the diffusion fluxes, J_i, the M–S formulation for n-component diffusion takes the form

$$-\frac{x_i}{RT}\frac{d\mu_i}{dz} = \sum_{j=1_{j\neq i}}^{n} \frac{x_jJ_i - x_iJ_j}{c_tĐ_{ij}}; \quad i = 1, 2, \ldots n \tag{3}$$

For mixtures of ideal gases, the Maxwell–Stefan formulation is entirely consistent with the kinetic theory of gases, and the pair diffusivities $Đ_{ij}$ can be identified with the diffusivity in the *binary* gas mixture of species i and species j.

Uphill diffusion in binary mixtures caused by phase splitting

For a binary mixture, Eq. (3) reduces to yield the following expression for the diffusion flux of species 1 in the mixture with species 2

$$J_1 = -c_tĐ_{12}\frac{x_1}{RT}\frac{d\mu_1}{dz} = -c_tĐ_{12}\frac{x_1}{RT}\left(\frac{\partial\mu_1}{\partial x_1}\right)\frac{dx_1}{dz} \tag{4}$$

Comparing with Eq. (1), we note that the Fick diffusivity is related to the M–S diffusivity

$$D_{12} = Đ_{12}\Gamma; \quad \Gamma \equiv \frac{x_1}{RT}\left(\frac{\partial\mu_1}{\partial x_1}\right) \tag{5}$$

For thermodynamically ideal mixtures, $\Gamma = 1$, and the Fick diffusivity can be identified with the M–S diffusivity. For mixtures of liquids, alloys, and glasses the tendency for phase separation has a strong influence on the Fick diffusivity, causing it to attain negative values and, as a consequence, the phenomenon of uphill transport. To demonstrate this possibility, let us consider diffusion in a binary alloy mixture consisting of Fe (= component 1) and Cr (= component 2). Let us combine n_{Fe} atoms of Fe and n_{Cr} atoms of Cr in a face centered cubic (FCC) lattice

with a total of N sites. The increase in entropy associated in this mixing process is given by the Boltzmann equation $S = k_B N_A \ln W = R \ln W$, where k_B is the Boltzmann constant, N_A is the Avagadro number, R is the gas constant, $R = k_B N_A$, and W is the total number of configurations by which the Fe and Cr atoms can be arranged within the FCC lattice: $W = N!/n_{Fe}!\, n_{Cr}!$. Use of Stirling's approximation for large number of sites, $\ln N! = N \ln N - N$, yields $S = -R(x_1 \ln x_1 + x_2 \ln x_2)$, where $x_1 = n_{Fe}/N$, and $x_2 = n_{Cr}/N$ are the atom fractions of Fe and Cr in the lattice. If the mixing process is thermodynamically ideal, the associated change in the Gibbs free energy is $G^{ideal} = -TS = RT(x_1 \ln x_1 + x_2 \ln x_2)$. Calculations of G^{ideal} are shown in Figure 2a, for $T = 800$ K, and $T = 1200$ K. The free energy is reduced on mixing Fe and Cr. For an ideal mixture, mixing in all proportions of Fe and Cr is favored at both 800 K and 1200 K because the free energy is lowered in the mixture.

The formation of mixtures of Fe and Cr atoms does not, however, occur in an ideal manner. The mixing process requires overcoming of the lattice strain energy and the formation of Fe-Cr bonds. The *excess* Gibbs free energy can be estimated using the regular solution model, $G^{ex} = RT(x_1 \ln \gamma_1 + x_2 \ln \gamma_2) = ARTx_1x_2$ where A is determined from experimental data [10]; the calculations are shown in Figure 2b. The total Gibbs free energy, $G = G^{ideal} + G^{excess}$, calculated for 800 K and 1200 K are shown in Figure 2c.

Figure 2

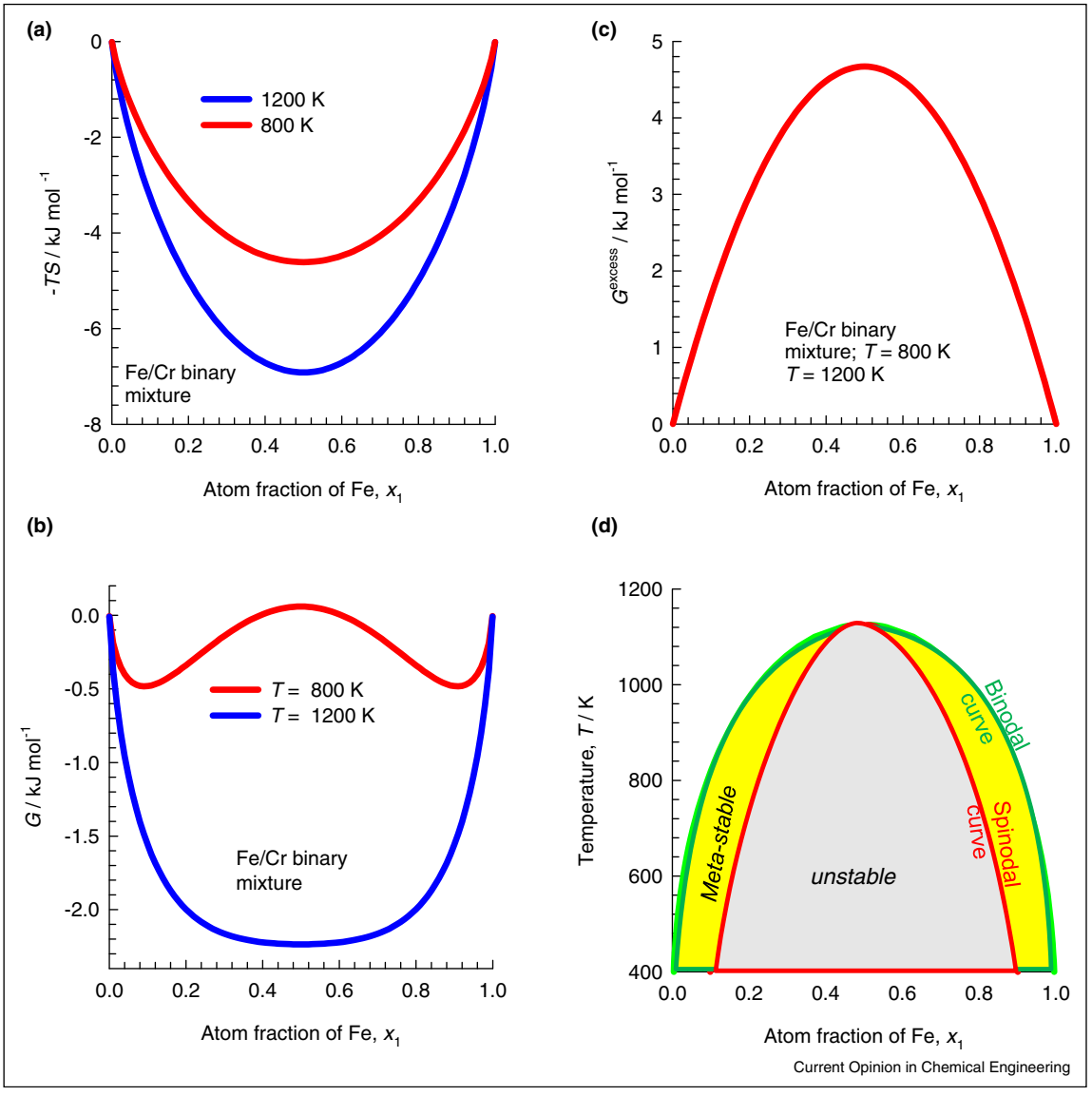

(a–c) Calculations of (a) $G^{ideal} = -TS$, (b) G^{excess}, and $G = G^{ideal} + G^{excess}$ for Fe(1)/Cr(2) binary alloy mixtures at 800 K, and 1200 K, as a function of the atom fraction of Fe (1). **(d)** Binodal and spinodal curves. The calculations are based on the data of Soriano-Vargas *et al.* [10].

At $T = 1200$ K, the free energy curve is "bow shaped", indicating that the mixtures are miscible in all proportions. However, we note that the free energy at 800 K, exhibits two minima corresponding to $\partial G/\partial x_1 = 0$; these minima occur at $x_1 = 0.09164$ and $x_1 = 0.90836$. Alloys of these two compositions are in equilibrium with each other. At $x_1 = 0.5$, the free energy exhibits a maximum, and represents an unstable state for the mixture. From the data on the vanishing of the first derivative $\partial G/\partial x_1 = 0$, we can determine the compositions of the two alloy phases that are in equilibrium with each other for various temperatures. The two points thus obtained at various values of temperature T, yields the binodal curve (indicated in green) in Figure 2d. The vanishing of the second derivative of the Gibbs free energy $\partial^2 G/\partial x_1^2 = \partial \mu_1/\partial x_1 = 0$ delineates the limits of phase instability and defines the spinodal curve. This requirement

Figure 3

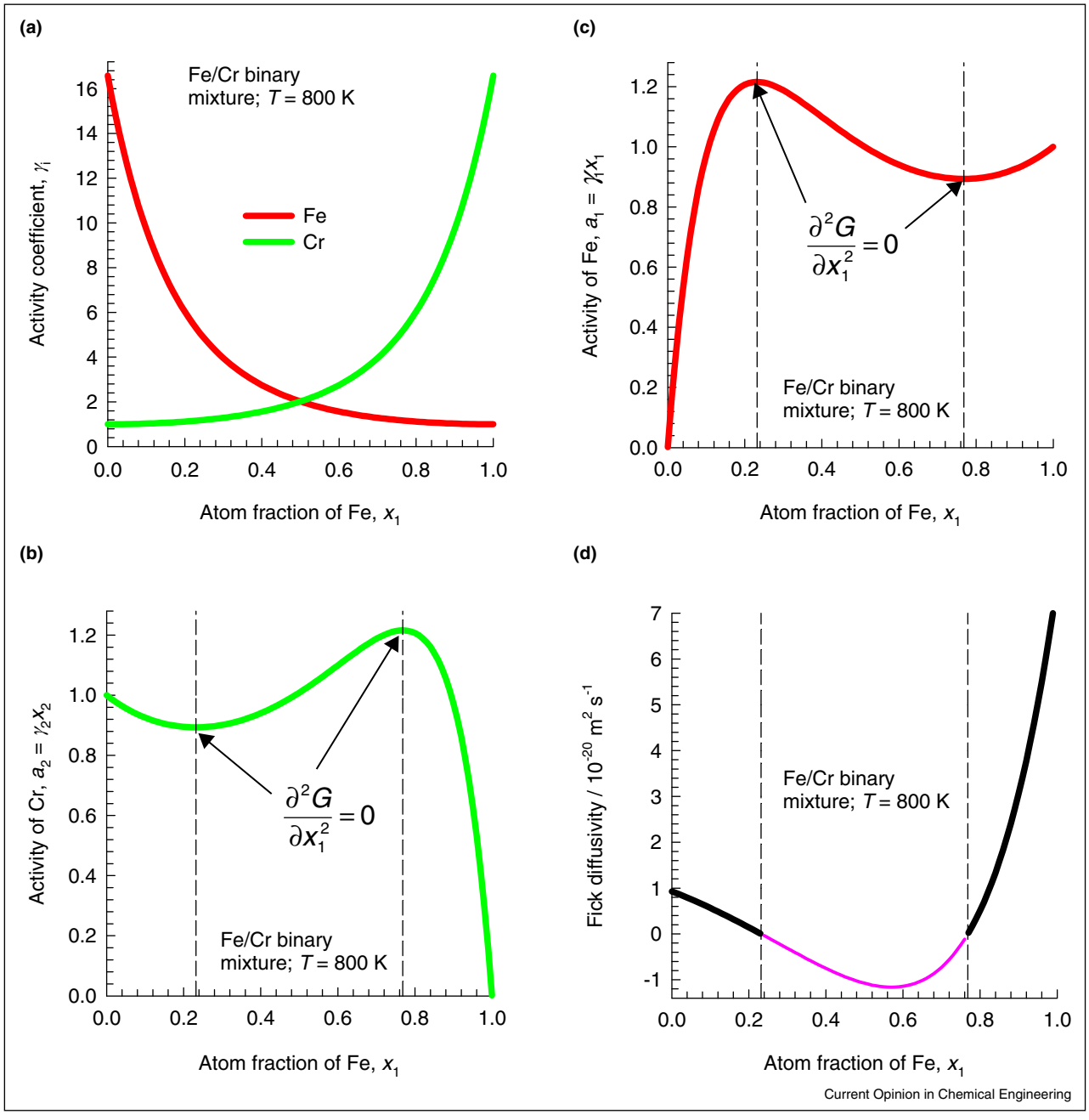

Calculations of **(a)** activity coefficients, γ_i, **(b)** activity of Fe (1), **(c)** activity of Cr (2), and Fick diffusivity for Fe(1)/Cr(2) binary alloys at 800 K, as a function of the atom fraction of Fe(1). The calculations are based on the data of Soriano-Vargas *et al.* [10].

implies that Fick diffusivity vanish along the spinodal compositions; Eq. (5) yields along the spinodal compositions

$$D_{12} = Đ_{12}\Gamma = 0 \tag{6}$$

In order to determine the directions of the fluxes of Fe and Cr, we need to determine activity coefficients, and activities. The activity coefficients, γ_i, of Fe(1) and Cr(2) in the regular solution, as a function of the atom fraction of Fe(1), can be calculated from $\ln\gamma_1 = Ax_2^2$; $\ln\gamma_2 = Ax_1^2$.; see Figure 3a. At either end of the composition range, the activity coefficients are 16.6, indicating a high ''escaping tendency''. A few atoms of Fe in a Cr-rich environment feel ''out of place'' and have a high escaping tendency. Similarly, a few atoms of Cr in a Fe-rich environment will have a high activity coefficient. Figure 3b, and c presents calculations of the thermodynamic activity, defined by $a_i = \gamma_i x_i$. Consider the variation of the activity of Fe (1) with increase in its atom fraction, x_1. For the range of compositions, $0 < x_1 < 0.232$, an increase in x_1 results in a corresponding increase in the activity a_1. However, for the range of compositions, $0.232 < x_1 < 0.768$, an increase in x_1 results in a corresponding *decrease* in the activity a_1. Analogous arguments hold for the activity of Cr atoms. This implies that mixtures with $0.232 < x_1 < 0.768$, the Fe atoms must equilibrate to the composition $x_1 = 0.90836$ at which the activity of Fe is at a minimum, that is, the diffusion is uphill in terms of atom fraction Fe. Correspondingly, Cr atoms will diffuse to Cr-rich phase with $x_1 = 0.232$ at which the activity of Cr is at a minimum.

For all compositions within the spinodal envelope, $0.232 < x_1 < 0.768$, we have $\Gamma < 0$, and consequently the Fick diffusivity $D_{12} < 0$. If we adopt the Fickian formulation for the diffusion flux of Fe, then the Fick diffusivity $D_{12} < 0$ within the spinodal envelope; see Figure 3d.

Crystallization processes operate near meta-stable and supersaturation regions; consequently, the phase equilibrium thermodynamics has a significant influence on the diffusivity and crystal growth. This is illustrated by the variation of the diffusivity of urea in aqueous solutions, as reported by Myerson and Senol [11]. The Fick diffusivity tends to near-zero values as the spinodal composition is approached; the strong concentration dependence of the Fick diffusivity is due to the thermodynamic factor correction, Γ.

It is common practice to use chemical potential differences between the supersaturated solution and the crystal

Figure 4

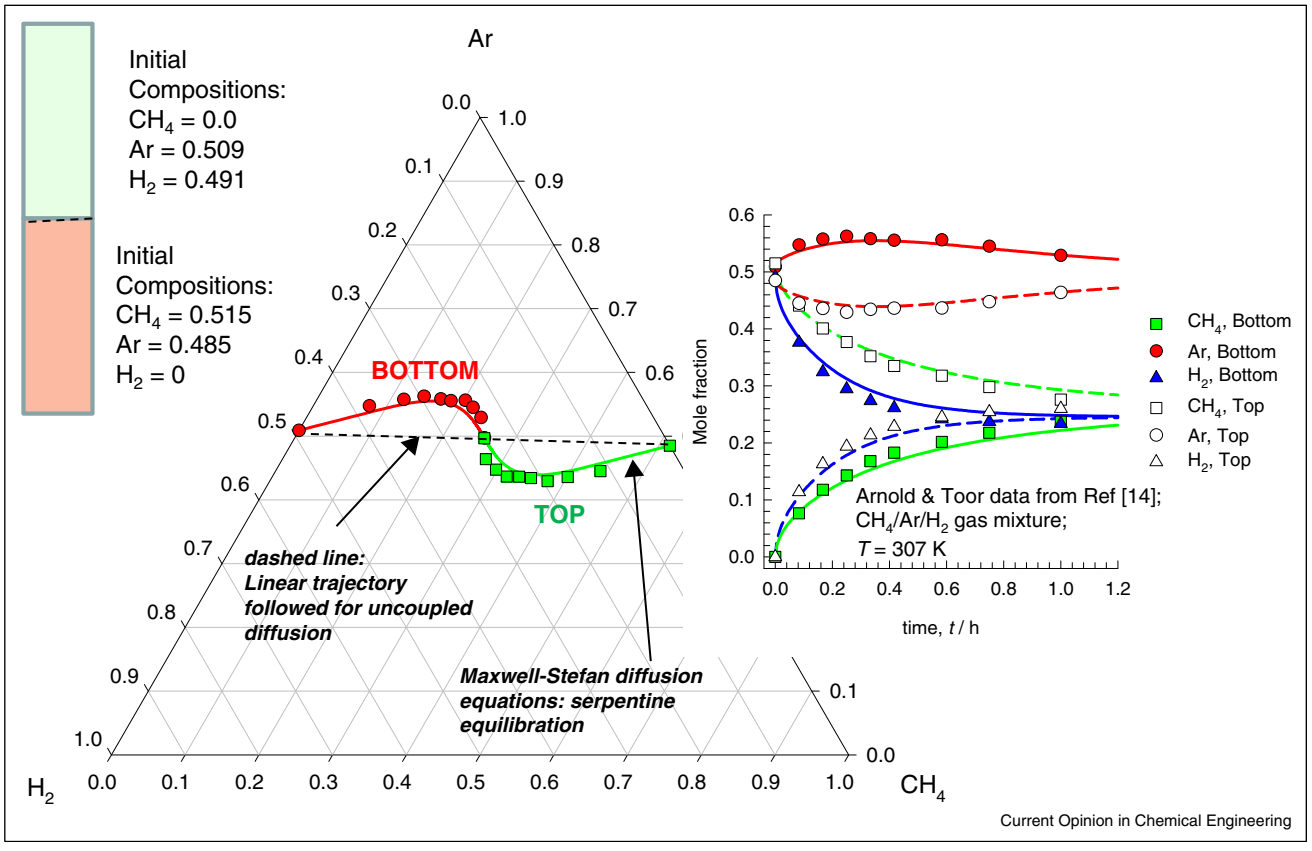

The Loschmidt tube experiment of Arnold and Toor [14] on the transient approach to equilibrium for $CH_4(1)/Ar(2)/H_2(3)$ gas mixtures. Further calculation details are provided by Krishna [9••].

$(\mu_i - \mu_{i,eq})/RT = \ln(a_i/a_{i,eq})$, as the driving force to model crystal growth kinetics [12,13].

Uphill diffusion in ternary mixtures of ideal gases

Consider the experimental data reported by Arnold and Toor [14] on the transient equilibration of $CH_4(1)/Ar(2)/H_2(3)$ gas mixtures of two different compositions in the top and bottom compartments of a Loschmidt tube; see Figure 4. The Loschmidt tubes are 12.7 mm in diameter and have a length, ℓ=0.406 m. The composition differences between the top and bottom compartments can be taken as the representative of the driving forces; the values are: $\Delta x_1 = -0.515$; $\Delta x_2 = 0.024$; $\Delta x_3 = 0.491$. We note that the driving force for Ar is significantly lower than that of its two partner species. The equilibration of CH_4, and H_2 occurs "normally"; the concentrations in the top and bottom compartment approach equilibrium, following an exponential decay. The transient equilibration of Ar, however, shows an overshoot (in bottom compartment) and an undershoot (in top compartment). In ternary composition space, the equilibration trajectories follow serpentine paths that imply the manifestation of uphill diffusion for Ar. Eq. (1) is unable to model the transient equilibration of Ar because it would require the diffusivity of argon to assume negative values for a time duration $0 < t < 0.3$ h.

Let us rationalize the experimental observations. For gaseous mixtures, there are no thermodynamic non-ideality influences and the chemical potential gradients are simply related to the gradients of the partial pressures $(1/RT)(d\mu_i/dz) = (1/p_i)(dp_i/dz)$. In the experiments, the total system pressure, $p_t = p_1 + p_2 + p_3$ is constant, and therefore $(1/RT)(d\mu_i/dz) = (1/x_i)(dx_i/dz)$. With this simplification, the Maxwell–Stefan (M–S) equations (3) reduces to yield a set of two independent equations

$$-\frac{dx_1}{dz} = \frac{x_2 J_1 - x_1 J_2}{c_t Đ_{12}} + \frac{x_3 J_1 - x_1 J_3}{c_t Đ_{13}}; \quad -\frac{dx_2}{dz} = \frac{x_1 J_2 - x_2 J_1}{c_t Đ_{12}} + \frac{x_3 J_2 - x_2 J_3}{c_t Đ_{23}} \tag{7}$$

We can recast Eq. (7) into the form of a generalized Fick's law using two-dimensional matrix notation

$$(J) = -c_t [D] \frac{d(x)}{dz} \tag{8}$$

The four elements of the Fick diffusivity matrix $[D]$ can be calculated explicitly from data on the M–S pair diffusivities

$$\begin{bmatrix} D_{11} & D_{12} \\ D_{21} & D_{22} \end{bmatrix} = \frac{\begin{bmatrix} Đ_{13}(x_1 Đ_{23} + (1-x_1)Đ_{12}) & x_1 Đ_{23}(Đ_{13} - Đ_{12}) \\ x_2 Đ_{13}(Đ_{23} - Đ_{12}) & Đ_{23}(x_2 Đ_{13} + (1-x_2)Đ_{12}) \end{bmatrix}}{x_1 Đ_{23} + x_2 Đ_{13} + x_3 Đ_{12}} \tag{9}$$

For the ternary $CH_4(1)/Ar(2)/H_2(3)$ gas mixture, the binary pair diffusivities are $Đ_{12} = 2.16 \times 10^{-5}$; $Đ_{13} = 7.72 \times 10^{-5}$; $Đ_{23} = 8.33 \times 10^{-5}$ m^2 s^{-1}. The differences in the pair diffusivities cause the off-diagonal elements of Fick matrix $[D]$ to be non-zero. At the equilibrated compositions $x_{1,eq} = 0.2575$, $x_{2,eq} = 0.4970$ and $x_{3,eq} = 0.2455$, we can determine the elements of the Fick matrix as $[D] = \begin{bmatrix} 4.44 & 1.83 \\ 3.64 & 6.3 \end{bmatrix} \times 10^{-5}$ m^2 s^{-1}. Particularly noteworthy is the large magnitude of the off-diagonal element D_{21}.

We can estimate the diffusion fluxes at time $t = 0$, using $(J) = -c_t[D](\Delta x)/\ell$. The diffusion fluxes are $J_1 = -2.19 \times 10^{-3}$, $J_2 = -1.69 \times 10^{-3}$, and $J_3 = 3.88 \times 10^{-3}$ mol m^{-2} s^{-1}. The fluxes of both $CH_4(1)$, and $Ar(2)$ are directed from the bottom compartment to the top compartment, whereas the flux of $H_2(3)$ is directed from the top compartment to the bottom compartment. Uphill diffusion of Ar (= component 2) occurs because the contribution of $D_{21}\Delta x_1 = -1.87 \times 10^{-5}$ is larger in magnitude and of opposite sign to the contribution of $D_{22}\Delta x_2 = 1.51 \times 10^{-6}$. Put another way, Ar is "dragged" uphill due to friction with the partner CH_4 molecules.

The transient overshoots and serpentine equilibration trajectories can be modeled quantitatively by solving the M–S equations (7), along with the equations of continuity [9••]; the simulation results are shown by the continuous and dashed lines in Figure 4. If the differences in the pair diffusivities are ignored, and the Fick matrix $[D]$ is taken to be a scalar (averaged) diffusivity times the identity matrix, then the equilibration trajectory in composition space is a straight line; no uphill diffusion is evidenced.

Is there a violation of the second law due to the phenomenon of uphill diffusion? For the ternary ideal gas mixture, the rate of entropy production is $\sigma = -R\sum_{i=1}^{n} J_i(1/x_i)(dx_i/dz)$. At the start of the experiment, we have $\sigma = R((J_1/x_1)(\Delta x_1/\ell) + (J_2/x_2)(\Delta x_2/\ell) + (J_3/x_3)(\Delta x_3/\ell))$. The individual contributions to the rate of entropy production are $\sigma_1 = 0.09$, $\sigma_2 = -1.67 \times 10^{-3}$, and $\sigma_3 = 0.159$ J m^{-3} s^{-1} K^{-1}. The rate of entropy production of $Ar(2)$ is negative, but the second law of thermodynamics is not violated because components $CH_4(1)$, and $H_2(3)$ produce entropy at such a rate to ensure that the total rate of entropy production remains positive definite, that is, $\sigma = \sigma_1 + \sigma_2 + \sigma_3 > 0$. A further point to note is that for ideal gas mixtures, the component activities are equal to the mole fractions; therefore, the transport of Ar is against its activity gradient during the initial stages of the diffusion equilibration.

The phenomenon of uphill diffusion in ternary gas mixtures is gainfully exploited in the application of heliox therapy to patients with chronic breathing difficulties [9••].

Diffusional coupling effects in multicomponent distillation

Distillation columns are normally designed using the equilibrium stage model [2•,15•,16••]; departures from equilibrium are accounted for by use of tray efficiencies. For a sieve tray column, for example, the contact time between the rising vapor bubbles and the surrounding liquid is finite and insufficient to attain the desired thermodynamic equilibrium value. The efficiency of contacting is described by Murphree efficiency, $E_i = (y_{iL} - y_{iE})/(y_{i,eq} - y_{iE})$ where y_{iE}, and y_{iL} are, respectively, the vapor phase mole fractions, entering and

Figure 5

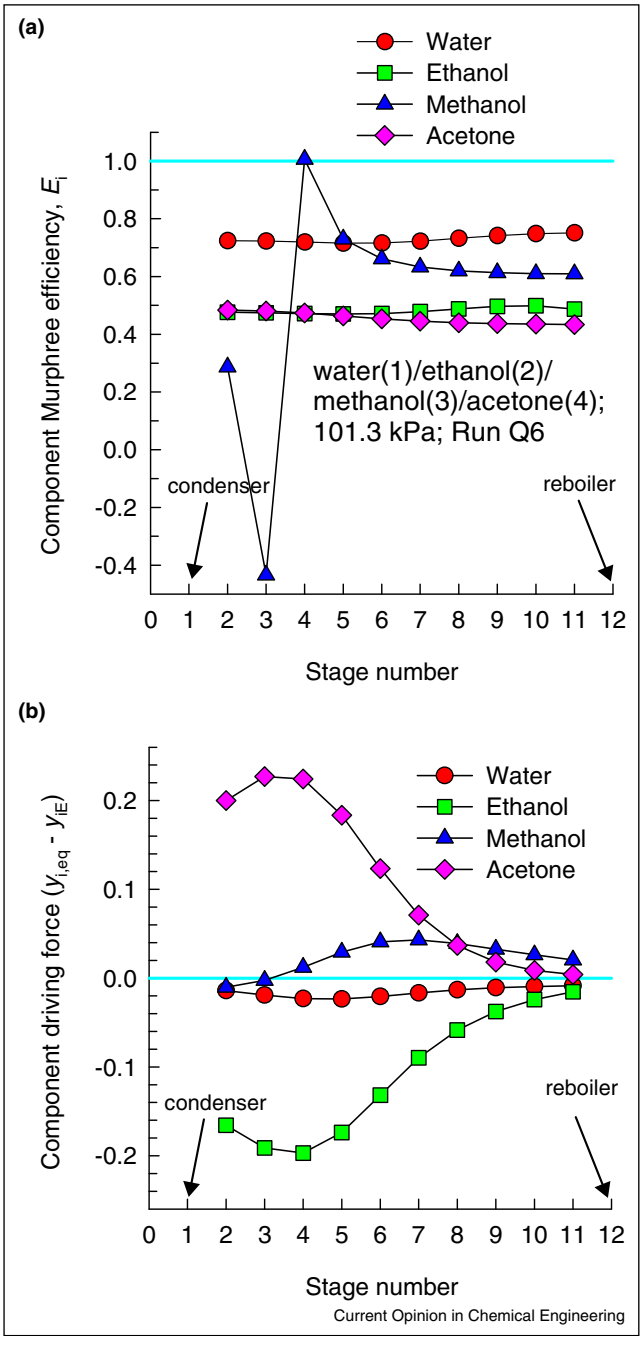

(a) Experimental data of Springer *et al.* [17••] for Murphree efficiencies for distillation of the quaternary water(1)/ethanol(2)/methanol(3)/acetone(4) mixtures in a 12-tray distillation column operating at total reflux. **(b)** Component driving forces on each stage.

leaving a tray, and $y_{i,eq}$ is the vapor composition in thermodynamic equilibrium with the liquid leaving the tray. For a tray in thermodynamic equilibrium, the component efficiencies are 100% for each component. For binary distillation, the Murphree component efficiencies are bounded, that is, $0 \leq E_1, = E_2 \leq 1$. For multicomponent distillation, with the number of species $n \geq 3$, coupled diffusion effects in either vapor or liquid phases cause the component efficiencies to be distinctly different from one another, $E_1 \neq E_2 \neq E_3 ... \neq E_n$. The phenomenon of uphill diffusion may lead to component efficiencies that exceed unity, $E_i > 1$ or have negative values, $E_i < 0$.

Experimental data of Springer *et al.* [17••] for distillation of the quaternary water(1)/ethanol(2)/methanol(3)/acetone(4) mixture in a 12-stage distillation column are presented in Figure 5a. The component Murphree efficiency of methanol is negative on stage 3, and slightly exceeds unity on stage 4. This implies that uphill diffusion of methanol manifests on stages 3 and 4. The rationalization is to be found in the fact that the driving force of methanol is practically zero on these two stages (see Figure 5b); the direction of transport of methanol is dictated by the transfer of the three partner species in the mixture: water, ethanol, and acetone. Methanol can be ''dragged'' uphill due to because of the larger fluxes of the partner species in the mixture. The classic Geddes model [18••] for equilibration of a spherical bubble rising through the froth dispersion on the tray can be used to quantify the uphill transport of methanol; the simulation details are provided in the Supplementary material.

Difference in the component Murphree efficiencies cause the column composition profiles to deviate significantly from that dictated by the residue curve maps (RCMs) that are widely used for examining feasible separation schemes for azeotropic mixtures [16••]. The RCMs describe the change of the composition of the liquid phase during continuous evaporation under conditions in which vapor-liquid equilibrium is maintained. As illustration, Figure 6 shows the composition profiles for distillation of the ternary mixture water(1)/ethanol(2)/acetone(3) in a sieve tray column operating at 101.3 kPa. Two different approaches are used in the calculation of the column profiles: (a) the conventional equilibrium stage model, and (b) the Maxwell–Stefan model to describe diffusion in both vapor and liquid phases. As expected, the equilibrium stage model predicts a column trajectory that follows the RCMs closely. However, the M–S model calculation, taking proper

Figure 6

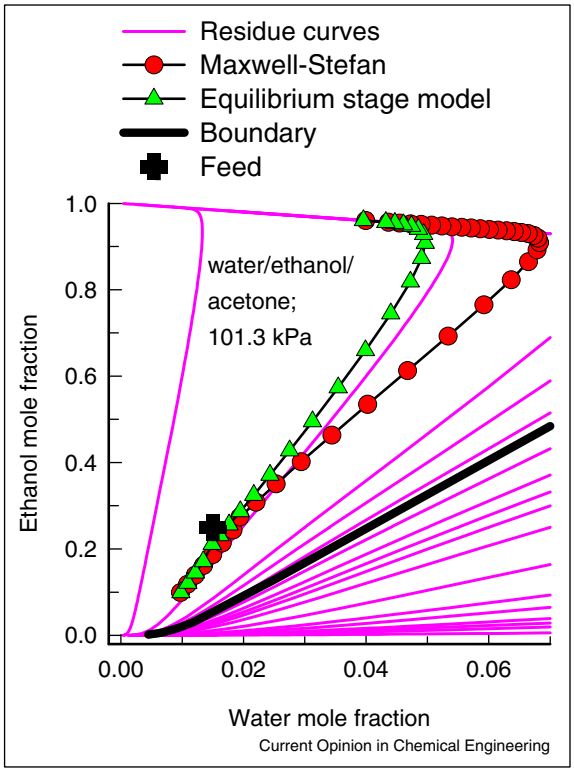

Composition profiles for sieve tray distillation column for the ternary mixture water(1)/ethanol(2)/acetone(3) at 101.3 kPa. Two different models are used to determine the composition profiles: the equilibrium stage model, and a non-equilibrium stage model using the Maxwell–Stefan diffusion equations [15•,19•].

account of diffusional coupling effects anticipates a curvilinear composition trajectory, deviating strongly from the RCM guidelines. For a specified purity of ethanol in the bottom product, significantly more number of stages will be required because of the ''scenic route'' followed by the tray compositions as it traverses down the column [15•,19•].

The phenomenon of uphill diffusion can be exploited to separate 2-propanol/water, ethanol/water, and acetone/methanol mixtures of azeotropic composition by distillation in the presence of an inert gas such as nitrogen, argon, or helium [19•,20,21]; this principle is explained by means of numerical examples in the Supplementary material.

Uphill diffusion in ternary mixtures of liquids and glasses

Diffusional coupling effects in multicomponent mixtures of liquids, alloys, and glasses are particularly strong. To analyze and quantify such effects it is useful to express the left member of Eq. (3) in terms of the mole fraction gradients by introducing an $(n-1)\times(n-1)$ matrix of thermodynamic factors $[\Gamma]$:

$$\frac{x_i}{RT}\frac{d\mu_i}{dz} = x_i\frac{d\ln a_i}{dz} = \sum_{j=1}^{n-1}\Gamma_{ij}\frac{dx_j}{dz}; \quad \Gamma_{ij} = \delta_{ij} + x_i\frac{\partial \ln \gamma_i}{\partial x_j}; \quad i,j = 1,2\ldots n{-}1 \tag{10}$$

The elements of $[\Gamma]$ can be calculated from UNIQUAC or NRTL models describing phase equilibrium thermodynamics [8••,19•]. For ternary mixtures, the Fick diffusivity matrix $[D]$, defined by Eq. (8), can be expressed explicitly as a product of two matrices

$$\begin{bmatrix} D_{11} & D_{12} \\ D_{21} & D_{22} \end{bmatrix} = \frac{\begin{bmatrix} Đ_{13}(x_1Đ_{23} + (1-x_1)Đ_{12}) & x_1Đ_{23}(Đ_{13}-Đ_{12}) \\ x_2Đ_{13}(Đ_{23}-Đ_{12}) & Đ_{23}(x_2Đ_{13} + (1-x_2)Đ_{12}) \end{bmatrix}}{x_1Đ_{23} + x_2Đ_{13} + x_3Đ_{12}} \begin{bmatrix} \Gamma_{11} & \Gamma_{12} \\ \Gamma_{21} & \Gamma_{22} \end{bmatrix} \tag{11}$$

For the glycerol(1)/acetone(2)/water(3) mixtures at the composition $x_1 = 0.1$, $x_2 = 0.3$, $x_3 = 0.6$ we calculate $[\Gamma] = \begin{bmatrix} 1.49 & 0.47 \\ 0.74 & 0.41 \end{bmatrix}$. The large off-diagonal elements of $[\Gamma]$ rationalize the large magnitudes of the off-diagonal elements of the Fick matrix $[D] = \begin{bmatrix} 0.4513 & 0.1618 \\ 0.2512 & 0.3075 \end{bmatrix} \times 10^{-9}\ \mathrm{m^2\ s^{-1}}$, that has been determined experimentally [22–24]. In order to demonstrate that the coupling effects in the Fick diffusivity matrix have their origins in the thermodynamic non-ideality effects, Figure 7 presents a plot of the ratio $(D_{12}D_{21})/(D_{11}D_{22})$ as a function of the ratio $(\Gamma_{12}\Gamma_{21})/(\Gamma_{11}\Gamma_{22})$. We see a unique dependence between the two sets of data. Along the spinodal curve, both of these ratios tend to unity values because the spinodal curve defines the stability limit, with $\Gamma = 0$, and $|D|=0$. The important message emerging from Figure 7 is that diffusional coupling effects become of increasing importance as the compositions approach values corresponding to the spinodal curve. Liquid extraction separations invariably operate close to composition regions corresponding to liquid–liquid phase splitting. Consequently, the phase equilibrium thermodynamics have a significant influence on the separation performance [19•].

Strong diffusional coupling effects in the vicinity of the phase-splitting regions cause the diffusion equilibration trajectories to be serpentine in shape, allowing the possibility of forays into the meta-stable regions. As illustration, let us examine the trajectory followed during equilibration of homogenous mixtures of two different compositions for the system water(1)/DMSO(2)/THF(3). A compartment with pure water is allowed to inter-diffuse with an adjacent compartment with the composition $x_1 = 0.25$, $x_2 = 0.42$ and $x_{3,\mathrm{eq}} = 0.33$. The composition of the equilibrated mixture is $x_{1,\mathrm{eq}} = 0.625$, $x_{2,\mathrm{eq}} = 0.21$ and $x_{3,\mathrm{eq}} = 0.165$, which point lies in the homogeneous region above the binodal curve. At the equilibrium composition, the thermodynamic factors are $[\Gamma] = \begin{bmatrix} 1.61 & -3.53 \\ -1.36 & 3.77 \end{bmatrix}$; the large off-diagonal elements cause the uphill diffusion of DMSO. We also note that the serpentine trajectory has penetrated the binodal envelope; see Figure 8. This indicates the spontaneous emulsification is feasible. The formation of emulsions by inter-diffusion of two homogeneous liquid mixtures of different compositions is termed the Ouzo effect [25]. The Ouzo effect can be exploited to form nanospheres without energy expenditure because the mixing is induced by inter-diffusion [26].

Serpentine diffusional equilibration trajectories, and transient overshoots are commonly encountered in mixtures of alloys, glasses and cements [5•,27,28,29•]; this is well illustrated by the experiments of Varshneya and Cooper [27]. Two glass slabs with different compositions of $K_2O(1)/SrO(2)/SiO_2(3)$ are brought into contact at time $t = 0$ and the transient concentration distributions determined in the each slab. The wt% of each component, measured at $t = 4.55$ h after the start of the experiment are shown in Figure 9. The over-shoot and under-shoot in the SrO concentrations signal the phenomenon of uphill diffusion; these are adequately modeled with the Fick matrix $[D] = \begin{bmatrix} 1 & -0.267 \\ -1.22 & 0.33 \end{bmatrix} \times 10^{-13}\ \mathrm{m^2\ s^{-1}}$. If the matrix of Fick diffusivities is assumed to be diagonal, the corresponding linear equilibration trajectories are indicat-

Figure 7

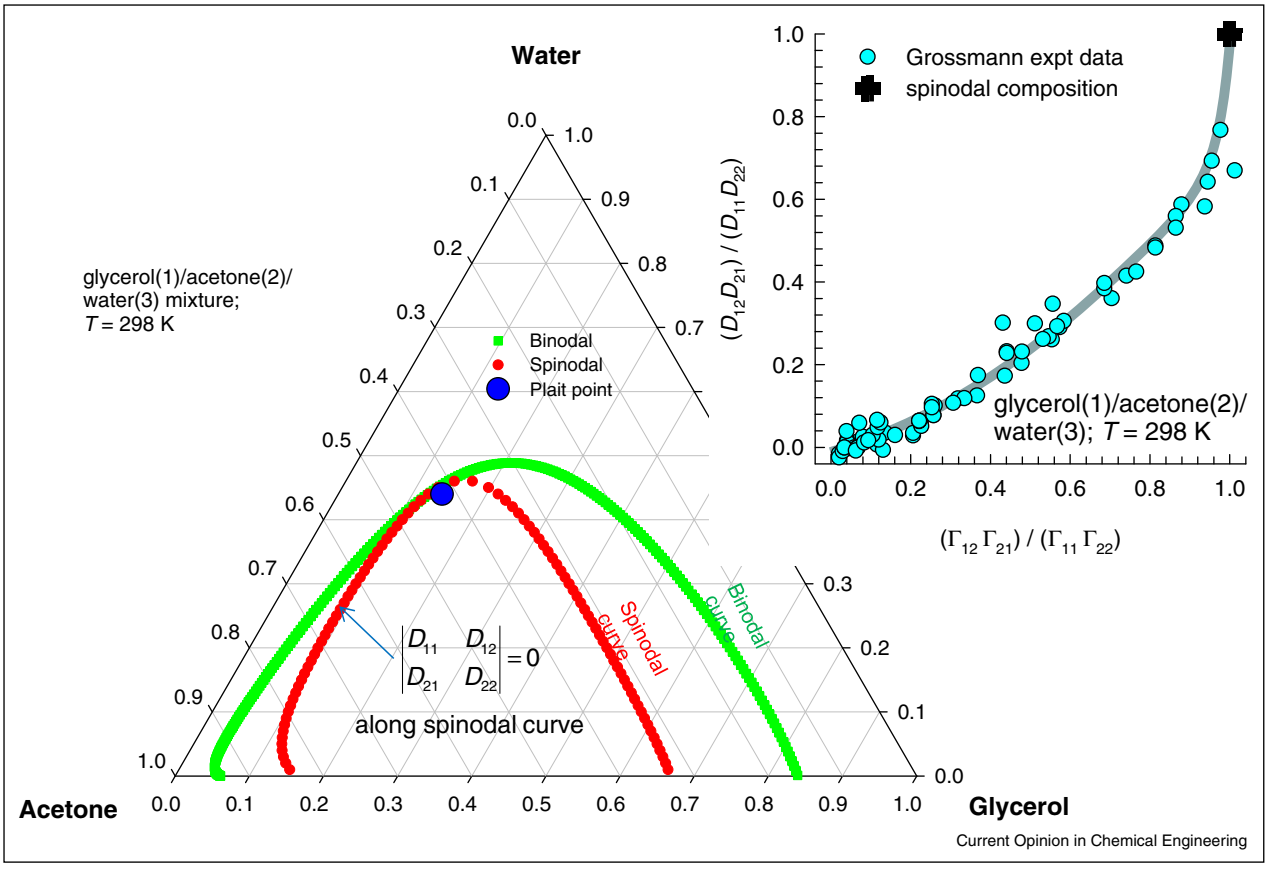

The phase equilibrium diagram for glycerol(1)/acetone(2)/water(3) mixtures at 298 K [42]. The ratio $(D_{12}D_{21})/(D_{11}D_{22})$ is plotted a function of the ratio $(\Gamma_{12}\Gamma_{21})/(\Gamma_{11}\Gamma_{22})$.

ed by the dashed lines in Figure 9. Uphill diffusion can be gainfully exploited to modify the surface properties of alloys and glasses.

Uphill diffusion in microporous adsorbents

Microporous materials such as activated carbon, zeolites, and metal organic frameworks (MOFs) are used as adsorbents in fixed beds, and as thin layers in membrane constructs [30•,31••,32]. The guest molecules are in the adsorbed phase. The force acting per mole of adsorbate species i is balanced by, firstly, friction between i and the pore walls, and secondly, friction between species i and species j. The extension of the M–S equation (2) is intuitive

$$-\frac{1}{RT}\frac{d\mu_i}{dz} = \sum_{j=1_{j\neq i}}^{n} \frac{x_j}{Đ_{ij}}(u_i - u_j) + \frac{1}{Đ_{i,w}}(u_i); \quad i = 1, 2 \ldots n \tag{12}$$

The x_i in equations (12) represent the component mole fractions in the adsorbed phase within the pores

$$x_i = \frac{q_i}{q_t}; \quad q_t = \sum_{i=1}^{n} q_i; \quad i = 1, 2, \ldots n \tag{13}$$

where q_i is the molar loading of the adsorbate. The $Đ_{i,w}$ quantify molecule-wall interactions; they may be interpreted as inverse drag coefficients between the species i and the material surface. For meso-porous and macroporous materials, the $Đ_{i,w}$ may be identified with the Knudsen diffusivity if the guest molecules have poor adsorption strength [33•]. The $Đ_{ij}$ may be interpreted as the inverse drag coefficient between species i and species j. At the molecular level, the $Đ_{ij}$ reflect how the facility for transport of species i *correlates* with that of species j; they are also termed *exchange coefficients*. For mesoporous and macroporous materials, the $Đ_{ij}$ can be identified with the corresponding diffusivity of the bulk fluid mixture [33•,34,35]. The multiplication factor x_j has been introduced in the numerator of the first right member of Eq. (12) because the friction experienced by species i with the each of the other species in the adsorbed phase should be proportional to the relative amounts of species j in the adsorbed phase.

If we define the fluxes in a reference velocity frame with respect to the pore walls, $N_i = \rho q_i u_i$, we derive [34]

Figure 8

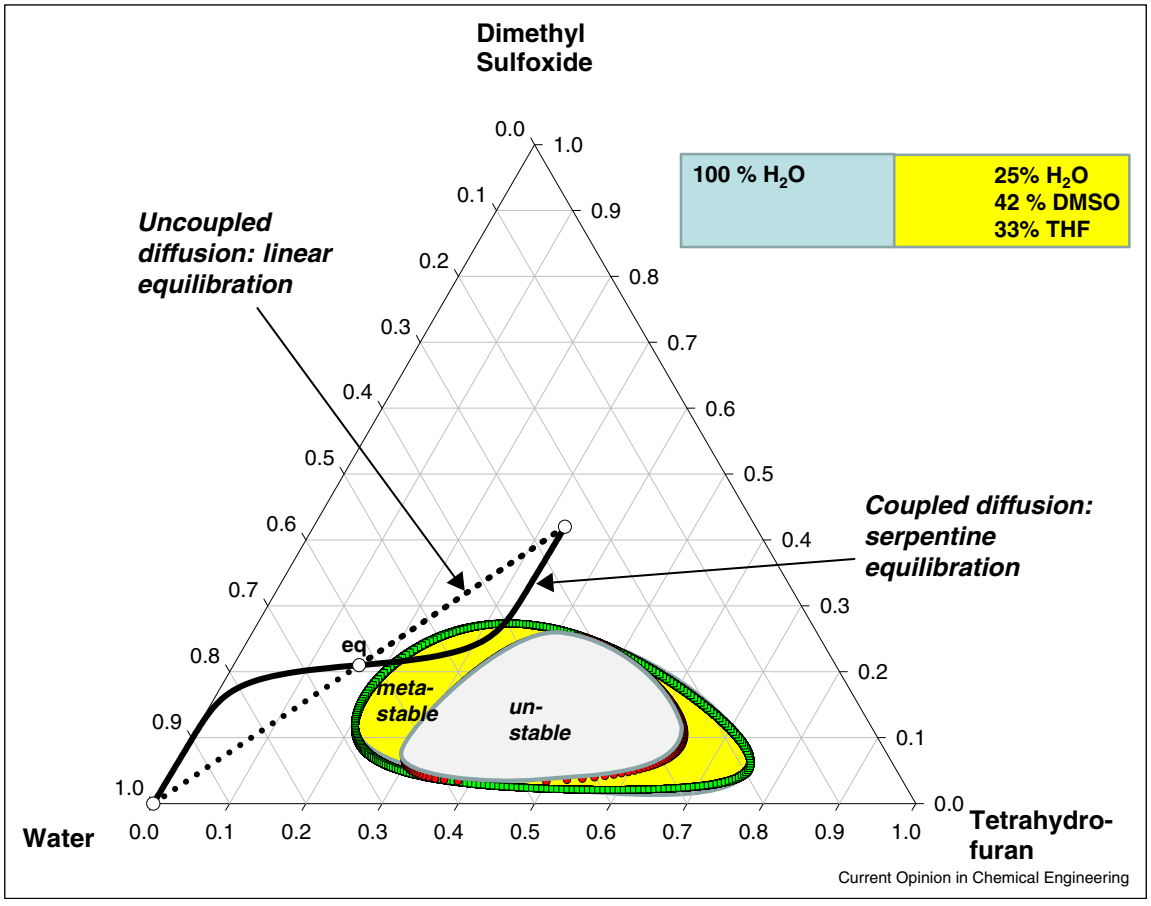

Trajectory followed during equilibration of homogenous mixtures of two different compositions for the system water(1)/DMSO(2)/THF(3); the equilibrium composition $x_{1,eq} = 0.625$, $x_{2,eq} = 0.21$ and $x_{3,eq} = 0.165$. DMSO = dimethyl sulfoxide; THF = tetrahydrofuran. Further calculation details are provided by Krishna [25].

$$-\rho\frac{q_i}{RT}\frac{d\mu_i}{\partial z} = \sum_{j=1_{j\neq i}}^{n}\left(\frac{x_j N_i - x_i N_j}{Đ_{ij}}\right) + \frac{N_i}{Đ_{i,w}}; \quad i = 1, 2\ldots n \tag{14}$$

Coupling effects for mixture diffusion in micropores is always important because the chemical potential of a component in the bulk fluid phase is dependent on the component loadings of all of the components in the adsorbed phase within the micropores. Such coupling effects often lead to uphill diffusion. The earliest experimental demonstration of uphill diffusion in microporous materials is reported in the classic paper of Habgood [36] for transient uptake of $N_2(1)/CH_4(2)$ mixtures is microporous LTA-4A zeolite. The uptake, measured at 194 K with partial pressures $p_1 = 10$ kPa and $p_2 = 90$ kPa, are shown in Figure 10. The $N_2(1)/CH_4(2)$ mixture constitutes a combination of more-mobile-less-strongly-adsorbed-N_2 and tardier-more-strongly-adsorbed-CH_4. Nitrogen is a ''pencil-like'' molecule (4.4 Å × 3.3 Å) that can hop length-wise across the narrow windows of LTA-4A; the ''spherical'' CH_4 (3.7 Å) is much more severely constrained and has a diffusivity that is about an order of magnitude lower than that of N_2. N_2 has an adsorption strength that is lower than that of CH_4. During the initial stages of the transient uptake, the pores of LTA-4A are predominantly richer in the more mobile N_2, but this is displaced by the more strongly-adsorbed-but-tardier CH_4 molecules at longer times. This results in an overshoot in the N_2 uptake. Note that the maximum loading of N_2 is about a factor five times that of the final equilibrated uptake. Put another way, supra-equilibrium loadings are attained for N_2 during a short time interval in the early stages of the transient uptake. The observed overshoot of N_2 can be modeled quantitatively using the M–S equation (14), taking proper account of (coupled) mixture adsorption equilibrium [31••]. Uphill diffusion of N_2 can be exploited to develop a process for purification of natural gas to meet pipeline specifications by selective uptake of N_2 that reduces the heating value.

The experimental data of Chen *et al.* [37] for transient uptake of O_2/N_2 mixture within a carbon molecular sieve

Figure 9

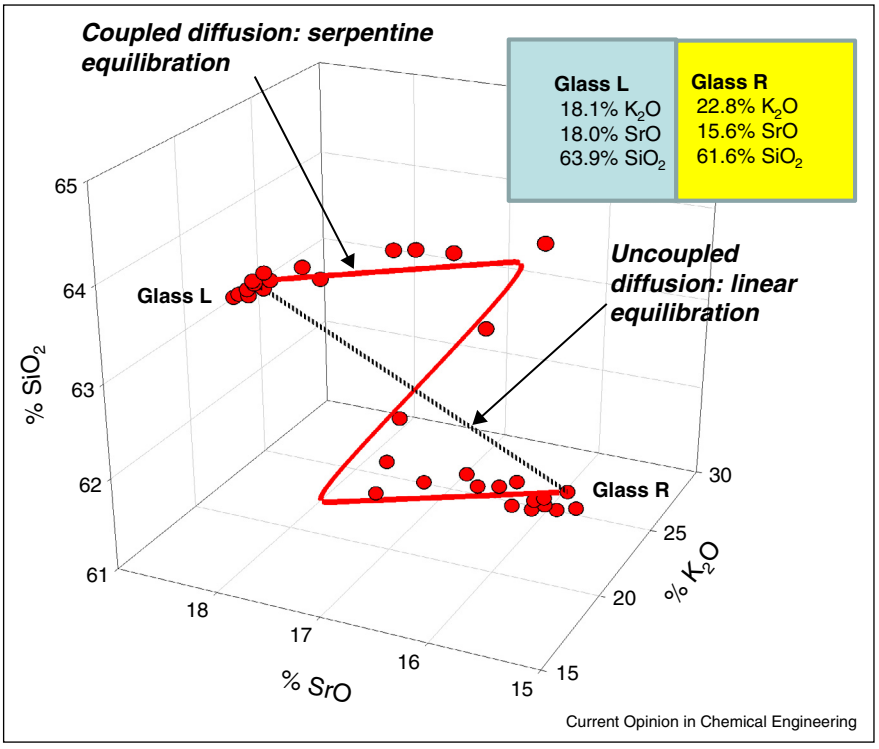

Experimental data of Varshneya and Cooper [27] for inter-diffusion between the left and right slabs consisting of $K_2O/SrO/SiO_2$ mixtures. The wt% of each component is measured on either side of the Matano plane, measured at $t = 4.55$ h after the start of the experiment are shown. Further calculation details are provided by Krishna [9••].

Figure 10

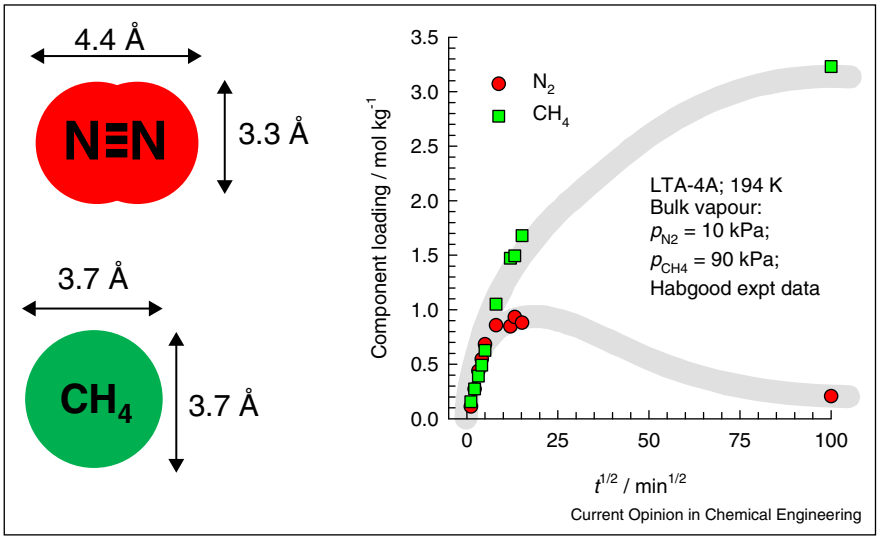

Experimental data of Habgood [36] on transient uptake of $N_2(1)/CH_4(2)$ mixture within LTA-4A crystals, exposed to binary gas mixtures at 194 K and partial pressures $p_1 = 10$ kPa; $p_2 = 90$ kPa.

particles shows an overshoot in the transient uptake of the more mobile O_2; such overshoots can be exploited to adsorb O_2 selectively from air using fixed bed adsorption units.

Conclusions

The following major conclusions can be drawn from the foregoing discussions and analysis.

(1) Coupling effects in mixture diffusion are often significant, and may cause uphill transport of a species against its concentration gradient. Transient overshoots, and serpentine equilibration trajectories in composition space are fingerprints of uphill diffusion.
(2) Diffusion in the vicinity of phase transition region for mixtures of liquids, metals, alloys, and glasses is strongly influenced by the constraints imposed by thermodynamic phase stability. Serpentine diffusion trajectories may enter meta-stable zones causing emulsification.
(3) Uphill diffusion strongly influences composition profiles in distillation columns, and may be exploited to break azeotropes by deliberate introduction of an inert gas.
(4) For transient uptake of mixtures within a microporous adsorbent, overshoots in loading of the more mobile partner species may occur; these are traceable to the influence of the influence of mixture adsorption thermodynamics. Transient overshoot phenomena may be exploited in diffusion-selective separations.
(5) The Maxwell–Stefan diffusion equations, with roots in irreversible thermodynamics, are the most convenient formulation to use for flux calculations. It is heartening to note that the modern texts on transport phenomena and separations include discussions on the M–S diffusion formulation [2•,8••,38•,39•,40•,41•].

Notation

a_i component activity, dimensionless
c_t total molar concentration of mixture, mol m^{-3}
D Fick diffusivity for binary mixture, $m^2\ s^{-1}$
$[D]$ Fick diffusivity matrix, $m^2\ s^{-1}$
$|D|$ Determinant of the Fick diffusivity matrix, $m^4\ s^{-2}$
$Đ_{i,w}$ diffusivity characterizing molecule-wall interactions, $m^2\ s^{-1}$
$Đ_{ij}$ M–S diffusivity, $m^2\ s^{-1}$
G Gibbs free energy, J mol^{-1}
G^{excess} Excess Gibbs free energy, J mol^{-1}
J_i molar diffusion flux of species i with respect to u, mol $m^{-2}\ s^{-1}$
k_B Boltzmann constant, 1.38×10^{-23} J $molecule^{-1}$ K^{-1}
ℓ Length of Loschmidt tube, m
n number of species in the mixture, dimensionless
N_A Avagadro number, 6.02×10^{23} molecules mol^{-1}
N_i molar flux of species i with respect to zeolite framework, mol $m^{-2}\ s^{-1}$
p_i partial pressure of species i in mixture, Pa
p_t total system pressure, Pa
q_i component molar loading of species i, mol kg^{-1}
q_t total molar loading in mixture, mol kg^{-1}
R gas constant, 8.314 J mol^{-1} K^{-1}
S entropy, J mol^{-1} K^{-1}
t time, s
T absolute temperature, K
x_i mole fraction of component i, dimensionless
u_i velocity of diffusion of species i, m s^{-1}
u molar average mixture velocity, m s^{-1}
z direction coordinate, m

Greek letters

γ_i activity coefficient of component i, dimensionless
$[\Gamma]$ matrix of thermodynamic factors, dimensionless
$|\Gamma|$ determinant of $[\Gamma]$, dimensionless
μ_i molar chemical potential of component, J mol^{-1}
ρ framework density of adsorbent, kg m^{-3}
θ_i fractional occupancy of component i, dimensionless
σ rate of entropy production, J $m^{-3}\ s^{-1}\ K^{-1}$

Appendix A. Supplementary data

Supplementary data associated with this article can be found, in the online version, at http://dx.doi.org/10.1016/j.coche.2016.04.003.

References and recommended reading

Papers of particular interest, published within the period of review, have been highlighted as:

- • of special interest
- •• of outstanding interest

1. Cussler EL: *Diffusion: Mass Transfer in Fluid Systems*. edn 3. • Cambridge: Cambridge University Press;; 2007.
This is a popular textbook, containing a brief introduction to the M–S formulation.

2. Seader JD, Henley EJ, Roper DK: *Separation Process Principles*. • edn 3. New York: John Wiley; 2011.
Includes an introduction to the M–S formulation.

3. Treybal RE: *Mass-Transfer Operations*. edn 3. New York: McGraw-Hill; 1980.

4. Onsager L: **Theories and problems of liquid diffusion**. *Ann NY Acad Sci* 1945, **46**:241-265.

5. Darken LS: **Diffusion of carbon in austenite with a discontinuity** • **in composition**. *Trans AIME* 1949, **180**:430-438.
An oft-cited classic contribution on uphill transport.

6. Maxwell JC: **On the dynamical theory of gases**. *Philos Trans R Soc* 1866, **157**:49-88.

7. Stefan J: **Über das gleichgewicht und die bewegung** •• **insbesondere die diffusion von gasgemengen**. *Sitzber Akad Wiss Wien* 1871, **63**:63-124.

A remarkably prescient paper that anticipated uphill diffusion.

8. Taylor R, Krishna R: *Multicomponent Mass Transfer*. New York: John Wiley; 1993.
•• This is a comprehensive text on the theory and applications of the M–S equations.

9. Krishna R: **Uphill diffusion in multicomponent mixtures**. *Chem Soc Rev* 2015, **44**:2812-2836.
•• A comprehensive review on uphill diffusion.

10. Soriano-Vargas O, Avila-Davila EO, Lopez-Hirata VM, Dorantes-Rosales HJ, Gonzalez-Velazquez JL: **Spinodal decomposition in an Fe–32 at%Cr alloy during isothermal aging**. *Mater Trans JIM* 2009, **50**:1753-1757.

11. Myerson AS, Senol D: **Diffusion coefficients near the spinodal curve**. *AIChE J* 1984, **30**:1004-1006.

12. Louhi-Kultanen M, Kallas J, Partanen J, Sha Z, Oinas P, Palosaari S: **The influence of multicomponent diffusion on crystal growth in electrolyte solutions**. *Chem Eng Sci* 2001, **56**:3505-3515.

13. Garside J: **Industrial crystallization from solution**. *Chem Eng Sci* 1985, **40**:3-26.

14. Arnold KR, Toor HL: **Unsteady diffusion in ternary gas mixtures**. *AIChE J* 1967, **13**:909-914.

15. Taylor R, Krishna R, Kooijman H: **Real-world modeling of distillation**. *Chem Eng Prog* 2003, **99**:28-39.
• A commentary on distillation mass transfer modelling.

16. Doherty MF, Malone MF: *Conceptual Design of Distillation Systems*. New York: McGraw-Hill; 2001.
•• Details of residue curves and much more on distillation process design.

17. Springer PAM, van der Molen S, Baur R, Krishna R: **Experimental verification of the necessity to use the Maxwell–Stefan formulation in describing trajectories during azeotropic distillation**. *Chem Eng Res Des* 2002, **80**:654-666.

18. Geddes RL: **Local efficiencies of bubble-plate fractionators**. *Trans Am Inst Chem Eng* 1946, **42**:79-105.
•• This is a classic contribution with application in diverse areas.

19. Krishna R: **Highlighting diffusional coupling effects in ternary liquid extraction and comparisons with distillation**. *Ind Eng Chem Res* 2016, **55**:1053-1063.
• Analysis of coupling effects in liquid extraction and distillation.

20. Fullarton D, Schlünder EU: **Diffusion distillation — a new separation process for azeotropic mixtures — Part I: Selectivity and transfer efficiency**. *Chem Eng Process* 1986, **20**:255-263.

21. Singh N, Prasad R: **Experimental studies on the effect of inert gases on diffusion distillation of ethanol–water mixtures**. *J Chem Technol Biotechnol* 2011, **86**:1495-1500.

22. Grossmann T, Winkelmann J: **Ternary diffusion coefficients of glycerol + acetone + water by taylor dispersion measurements at 298.15 K**. *J Chem Eng Data* 2005, **50**:1396-1403.

23. Grossmann T, Winkelmann J: **Ternary diffusion coefficients of glycerol + acetone + water by Taylor dispersion measurements at 298.15 K. 2. Acetone-rich region**. *J Chem Eng Data* 2007, **52**:336-340.

24. Grossmann T, Winkelmann J: **Ternary diffusion coefficients of glycerol + acetone + water by Taylor dispersion measurements at 298.15 K. 3. Water-rich region**. *J Chem Eng Data* 2007, **52**:341-344.

25. Krishna R: **Serpentine diffusion trajectories and the Ouzo effect in partially miscible ternary liquid mixtures**. *Phys Chem Chem Phys* 2015, **17**:27428-27436.

26. Ganachaud F, Katz JL: **Nanoparticles and nanocapsules created using the Ouzo effect: spontaneous emulsification as an alternative to ultrasonic and high-shear devices**. *ChemPhysChem* 2005, **6**:209-216.

27. Varshneya AK, Cooper AR: **Diffusion in the system K_2O–SrO–SiO_2: III. Interdiffusion coefficients**. *J Am Ceram Soc* 1972, **55**:312-317.

28. Vielzeuf D, Saúl A: **Uphill diffusion, zero-flux planes and transient chemical solitary waves in garnet**. *Contrib Miner Petrol* 2011, **161**:683-702.

29. Glicksman ME: *Diffusion in Solids: Field Theory Solid-state Principles, and Applications*. New York: John Wiley; 2000.
• A standard text on diffusion in solids and metal alloys.

30. Krishna R: **Methodologies for evaluation of metal-organic frameworks in separation applications**. *RSC Adv* 2015, **5**:52269-52295.
• Applications of microporous adsorbents in separations.

31. Krishna R: **The Maxwell–Stefan description of mixture diffusion in nanoporous crystalline materials**. *Microporous Mesoporous Mater* 2014, **185**:30-50.
•• The M–S theory applied to nanoporous adsorbents and membranes.

32. Krishna R, van Baten JM: **Investigating the influence of diffusional coupling on mixture permeation across porous membranes**. *J Membr Sci* 2013, **430**:113-128.

33. Krishna R: **Investigating the validity of the Knudsen diffusivity prescription for mesoporous and macroporous materials**. *Ind Eng Chem Res* 2016, **55**:4749-4759 http://dx.doi.org/10.1021/acs.iecr.6b00762.
• Stresses the shortcomings of the dusty gas model for porous diffusion.

34. Krishna R, van Baten JM: **Unified Maxwell–Stefan description of binary mixture diffusion in micro- and meso-porous materials**. *Chem Eng Sci* 2009, **64**:3159-3178.

35. Krishna R, van Baten JM: **An investigation of the characteristics of Maxwell–Stefan diffusivities of binary mixtures in silica nanopores**. *Chem Eng Sci* 2009, **64**:870-882.

36. Habgood HW: **The kinetics of molecular sieve action. Sorption of nitrogen-methane mixtures by linde molecular sieve 4A**. *Can J Chem* 1958, **36**:1384-1397.

37. Chen YD, Yang RT, Uawithya P: **Diffusion of oxygen, nitrogen and their mixtures in Carbon Molecular-Sieve**. *AIChE J* 1994, **40**:577-585.

38. Wesselingh JA, Krishna R: *Mass Transfer in Multicomponent Mixtures*. Delft: VSSD; 2000.
• A primer on the M–S theory, with applications in separations and reactions.

39. Sirkar KK: *Separation of Molecules, Macromolecules and Particles. Principles Phenomena and Processes*. Cambridge: Cambridge University Press; 2014.
• A modern text on separations.

40. Bird RB, Stewart WE, Lightfoot EN: *Transport Phenomena*. edn 2. New York, USA: John Wiley; 2002.
• This updated edition contains an introduction to the M–S equations.

41. Wankat PC: *Separation Process Engineering*. edn 3. Upper Saddle River, New Jersey, USA: Prentice-Hall; 2012.
• A modern text on separations.

42. Krishna R, Low CY, Newsham DMT, Olivera Fuentes CG, Paybarah A: **Liquid liquid equilibrium in the system glycerol water acetone at 25 °C**. *Fluid Phase Equilib* 1989, **45**:115-120.

Supplementary material to accompany:

Diffusing Uphill with James Clerk Maxwell and Josef Stefan

Rajamani Krishna

Van 't Hoff Institute for Molecular Sciences, University of Amsterdam, Science Park 904,

1098 XH Amsterdam, The Netherlands

email: r.krishna@contact.uva.nl

Table of Contents

1. Preamble

The Supplementary material (*e*-content) accompanying the manuscript *Diffusing Uphill with James Clerk Maxwell and Josef Stefan* provides (a) Introduction and derivation of the Maxwell-Stefan equations, (b) Simulations to demonstrate the principle of diffusion distillation for separation of azeotropes, and (c) Geddes model simulations to demonstrate uphill transport of methanol in quaternary distillation of water(1)/ethanol(2)/methanol(3)/acetone(4) mixtures.

2. Introduction to the Maxwell-Stefan diffusion formulation

The approach we adopt to describe diffusion stems from the pioneering works of James Clerk Maxwell [1] and Josef Stefan [2] who analyzed diffusion in ideal gas mixtures. The Maxwell-Stefan (M-S) formulation is best understood by considering *z*-directional diffusion in a binary gas mixture consisting of species 1 and 2, contained within the control volume shown schematically in Figure 1. The cross-sectional area available for diffusion is 1 m^2 and the length of the diffusion path is dz. If the change in the partial pressure of component *i* across the diffusion distance dz is $-dp_i$, the force acting on species *i* per m^3 is $-\frac{dp_i}{dz}$. The number of moles of species *i* per m^3, $c_i = \frac{p_i}{RT}$, and therefore the force acting per mole of species *i* is $-\frac{RT}{p_i}\frac{dp_i}{dz}$ which for an ideal gas mixture at constant temperature also equals the chemical potential gradient $-\frac{d\mu_i}{dz}$. This force is balanced by friction between the diffusing species 1 and 2, each diffusing with a velocity u_i (cf. Figure 2). We may expect that the frictional drag to be proportional to the velocity difference $(u_1 - u_2)$, and we write $-\frac{d\mu_1}{dz} = \frac{RT}{Đ_{12}} x_2 (u_1 - u_2)$ where the term $\frac{RT}{Đ_{12}}$ is to be interpreted as the drag coefficient. The multiplier x_2 in the right member represents the mole fraction of component 2; this factor is introduced because we expect the friction to be dependent on the number of molecules of 2 relative to that of component 1. The Maxwell-Stefan diffusivity $Đ_{12}$

has the units m^2 s^{-1} and the physical significance of an inverse drag coefficient. The extension to *n*-component mixtures is intuitively obvious [3, 4]:

$$-\frac{1}{RT}\frac{d\mu_i}{dz}=\sum_{\substack{j=1\\ j\neq i}}^{n}\frac{x_j\left(u_i-u_j\right)}{Đ_{ij}};\quad i=1,2,\ldots n \tag{1}$$

The pair diffusivity $Đ_{ij}$ can be interpreted as an inverse "drag coefficient" between species *i* and species *j*. Equation (1) is consistent with the theory of irreversible thermodynamics. The Onsager

The Onsager reciprocal relations demand the symmetry constraint

$$Đ_{ij}=Đ_{ji};\quad i,j=1,2,\ldots n \tag{2}$$

For *n*-component ideal gas mixtures, the molar diffusion fluxes J_i are defined as

$$J_i\equiv c_i\left(u_i-u\right);\quad i=1,2,,,.n \tag{3}$$

are defined with respect to the chosen molar average reference velocity frame u

$$u=y_1u_1+y_2u_2+\ldots y_nu_n \tag{4}$$

Only *n*-1 of the fluxes J_i are independent because the diffusion fluxes sum to zero

$$\sum_{i=1}^{n-}J_i=0 \tag{5}$$

In terms of the diffusion fluxes, J_i, the M-S formulation for *n*-component diffusion takes the form

$$-\frac{x_i}{RT}\frac{d\mu_i}{dz}=\sum_{\substack{j=1\\ j\neq i}}^{n}\frac{x_jJ_i-x_iJ_j}{c_tĐ_{ij}};\quad i=1,2,\ldots n \tag{6}$$

For mixtures of ideal gases, $\frac{y_i}{RT}\frac{d\mu_i}{dz}=\frac{dy_i}{dz}$, and equation (6) simplifies to

$$-\frac{dy_i}{dz}=\sum_{\substack{j=1\\ j\neq i}}^{n}\frac{x_jJ_i-x_iJ_j}{c_tĐ_{ij}};\quad i=1,2,\ldots n \tag{7}$$

Equation (7) is entirely consistent with the kinetic theory of gases, and the pair diffusivities $Đ_{ij}$ can be identified with the diffusivity in the *binary* gas mixture of species *i* and species *j*.

Only *n*-1 of the Equations (7) are independent because the mole fractions sum to unity and the mole fraction gradients sum to zero

$$\sum_{i=1}^{n} y_i = 1; \quad \frac{dy_1}{dz} + \frac{dy_2}{dz} + ... \frac{dy_n}{dz} = 0 \tag{8}$$

Equations (7) are applicable also to situations in which there is a temperature gradient along the diffusion path; in this case the molar concentration of the mixture

$$c_t = \frac{p_t}{RT} \tag{9}$$

is to be evaluated at the average temperature in the diffusion layer.

For solving equations (7), it is convenient to re-cast these equations into (*n*-1) dimensional matrix notation

$$-c_t \frac{d(y)}{dz} = [B](J) \tag{10}$$

Where we define a (*n*-1) × (*n*-1) dimensional matrix of *inverse* diffusivities $[B]$ whose elements are given by

$$B_{ii} = \frac{x_i}{Đ_{in}} + \sum_{\substack{k=1 \\ k \neq i}}^{n} \frac{x_k}{Đ_{ik}}; \quad B_{ij(i \neq j)} = -x_i \left(\frac{1}{Đ_{ij}} - \frac{1}{Đ_{in}} \right); \quad i, j = 1,2...n-1 \tag{11}$$

Equations (10) may be re-written in (*n*-1) dimensional matrix notation

$$(J) = -c_t [D] \frac{d(y)}{dz} \tag{12}$$

The (*n*-1) × (*n*-1) dimensional Fick diffusivity matrix is

$$[D] = [B]^{-1} \tag{13}$$

For the solution of practical problems we need to calculate the molar fluxes N_i in the laboratory fixed reference frame; these are related to the diffusion fluxes J_i by

$$N_i \equiv c_i u_i = J_i + y_i N_t; \quad N_t = \sum_{i=1}^{n} N_i = \sum_{i=1}^{n} c_i u_i = c_t u \tag{14}$$

The determination of *n* fluxes N_i requires an additional relationship, called the *bootstrap* relation. The first example of the bootstrap relation is the condition of equimolar counter-diffusion

$$N_1 + N_2 + ...N_n = N_t = c_t u = 0 \tag{15}$$

For equimolar counter-diffusion, that is relevant for distillation operations (without inert gas) we have

$$N_i = J_i; \quad i = 1,2,..n \tag{16}$$

The bootstrap relation that is relevant to sweep gas distillation is the requirement that the inert gas (component *n*) does not transfer across the vapor/liquid interface into the liquid phase:

$$N_n = 0 \tag{17}$$

In this case, the molar fluxes N_i are linearly related to the diffusion fluxes by J_i

$$(N) = [\beta](J) \tag{18}$$

The elements of the bootstrap matrix are

$$\beta_{ij} = \delta_{ij} + \frac{y_i}{y_n}; \quad i, j = 1,2,,..n-1 \tag{19}$$

Krishna and Standart[5] have developed exact solutions to equation (7), combined with a bootstrap relation, either equation (16) or (18), for explicit evaluation of the fluxes for steady-state transfer across a film of thickness δ.

3. The Maxwell-Stefan formulation for diffusion in ternary ideal gas mixtures

For 3-component ideal gas mixtures, equations (7) reduce to

$$
\begin{aligned}
-\frac{dy_1}{dz} &= \frac{y_2 J_1 - y_1 J_2}{c_t Đ_{12}} + \frac{y_3 J_1 - y_1 J_3}{c_t Đ_{13}}; \\
-\frac{dy_2}{dz} &= \frac{y_1 J_2 - y_2 J_1}{c_t Đ_{12}} + \frac{y_3 J_2 - y_2 J_3}{c_t Đ_{23}} \\
-\frac{dy_3}{dz} &= \frac{y_1 J_3 - y_3 J_1}{c_t Đ_{13}} + \frac{y_2 N_3 - y_3 J_2}{c_t Đ_{23}}
\end{aligned}
\tag{20}
$$

The inversion of the matrix [B] can be performed explicitly and the 2 × 2 dimensional matrix [D] are explicitly related to the pair M-S diffusivities $Đ_{12}$, $Đ_{13}$, and $Đ_{23}$

$$
\begin{bmatrix} D_{11} & D_{12} \\ D_{21} & D_{22} \end{bmatrix} = \frac{\begin{bmatrix} Đ_{13}\left(y_1 Đ_{23} + (1-y_1) Đ_{12}\right) & y_1 Đ_{23}\left(Đ_{13} - Đ_{12}\right) \\ y_2 Đ_{13}\left(Đ_{23} - Đ_{12}\right) & Đ_{23}\left(y_2 Đ_{13} + (1-y_2) Đ_{12}\right) \end{bmatrix}}{y_1 Đ_{23} + y_2 Đ_{13} + y_3 Đ_{12}}
\tag{21}
$$

For distillation of components 1 and 2 in the presence of an inert gas (component 3), $N_3 = 0$. The elements of the 2 × 2 dimensional matrix $[\beta]$ can be determined explicitly

$$
[\beta] = \begin{bmatrix} 1 + \dfrac{y_1}{y_3} & \dfrac{y_1}{y_3} \\ \dfrac{y_2}{y_3} & 1 + \dfrac{y_2}{y_3} \end{bmatrix}
\tag{22}
$$

Combining equations (12), (18), (21), and (22), we obtain

$$
\begin{pmatrix} N_1 \\ N_2 \end{pmatrix} = -c_t \begin{bmatrix} 1 + \dfrac{y_1}{y_3} & \dfrac{y_1}{y_3} \\ \dfrac{y_2}{y_3} & 1 + \dfrac{y_2}{y_3} \end{bmatrix} \frac{\begin{bmatrix} Đ_{13}\left(y_1 Đ_{23} + (1-y_1) Đ_{12}\right) & y_1 Đ_{23}\left(Đ_{13} - Đ_{12}\right) \\ y_2 Đ_{13}\left(Đ_{23} - Đ_{12}\right) & Đ_{23}\left(y_2 Đ_{13} + (1-y_2) Đ_{12}\right) \end{bmatrix}}{y_1 Đ_{23} + y_2 Đ_{13} + y_3 Đ_{12}} \begin{pmatrix} \dfrac{dy_1}{dz} \\ \dfrac{dy_2}{dz} \end{pmatrix}
\tag{23}
$$

For analysis of sweep-gas distillation we use the simplified procedure suggested by Krishna[6]. We evaluate both the matrices $[\beta]$ and $[D]$ at the arithmetic average vapor compositions in the $y_i = \dfrac{y_{i0} + y_{i\delta}}{2}$. With this simplification, the fluxes can be evaluated explicitly as follows

$$\begin{pmatrix} N_1 \\ N_2 \end{pmatrix} = \frac{c_t}{\delta} \begin{bmatrix} 1+\frac{y_1}{y_3} & \frac{y_1}{y_3} \\ \frac{y_2}{y_3} & 1+\frac{y_2}{y_3} \end{bmatrix} \frac{\begin{bmatrix} Đ_{13}\left(y_1 Đ_{23}+(1-y_1)Đ_{12}\right) & y_1 Đ_{23}\left(Đ_{13}-Đ_{12}\right) \\ y_2 Đ_{13}\left(Đ_{23}-Đ_{12}\right) & Đ_{23}\left(y_2 Đ_{13}+(1-y_2)Đ_{12}\right) \end{bmatrix}}{y_1 Đ_{23}+y_2 Đ_{13}+y_3 Đ_{12}} \begin{pmatrix} y_{10}-y_{1\delta} \\ y_{20}-y_{2\delta} \end{pmatrix} \tag{24}$$

4. Steady-state diffusional evaporation/condensation of ethanol/water/nitrogen

For a binary mixture, the vapor-liquid equilibrium is described by

$$y_i = \frac{\gamma_i x_i P_i^0}{p_t} \tag{25}$$

At the azeotropic composition, we have

$$y_i = x_i \tag{26}$$

Binary mixtures of azeotropic composition cannot be separated by distillation because there is no driving force for transfer from liquid to vapor phase.

If an inert gas, such as nitrogen, is introduced into the vapor phase, this allows mixtures of azeotropic composition to be separated because the vapor compositions are altered and driving forces for transfers are "created'. Diffusional effects can be exploited to separate alcohol/water mixtures of azeotropic composition by distillation in the presence of an inert gas such as nitrogen, argon, or helium.[7, 8] The principle of separation is illustrated by means of illustrative examples based on the solution of the Maxwell-Stefan equations.

As an illustration let us consider mass transfer between the liquid and vapor phase for ethanol(1)/water(2)/nitrogen(3). Figure 3 shows a schematic showing liquid/vapor transfer for ethanol (1) / water (2) /nitrogen (3). The mass transfer resistance is assumed to be restricted to the vapor phase, and the effective film thickness of the gas phase resistance is $\delta = 1$ mm.

We first consider diffusional evaporation as a strategy for breaking the ethanol/water azeotrope.

Assume that the liquid phase is the binary mixture ethanol(1)/water(2) at T = 343.15 K. The azeotropic composition at this temperature can be calculated as x_1 = 0.869, x_2 = 0.131; the calculations

are based on the NRTL parameters provided in Table 1. Let us bring this liquid phase in contact with an inert gas phase consisting of the nitrogen (= species 3). The vapor pressure of ethanol at 343.15 K is 71.2 kPa, and the vapor pressure of water at 343.15 K is 31.2 kPa. The total gas phase pressure p_t =101.3 kPa. The composition of the vapor phase at the gas/liquid interface in equilibrium with the liquid mixture can be calculated from $y_{i0} = \frac{\gamma_i x_i P_i^0}{p_t}$. This yields $y_{1\delta} = 0.6177$, $y_{2\delta} = 0.09264$, $y_{3\delta} = 0.28971$; see Figure 3. The bulk vapor composition is taken to be: $y_{10} = 0.0$, $y_{20} = 0.0$, $y_{30} = 1.0$.

The driving forces are $\Delta y_1 = y_{10} - y_{1\delta} = -0.6177$, and $\Delta y_2 = y_{1o} - y_{2\delta} = -0.09264$. Both driving forces are directed from liquid to the vapor phase. The ratio of driving forces $\frac{\Delta y_1}{\Delta y_2} = 6.67$.

The values of the vapor phase M-S diffusivities of the three binary pairs at 343.15 K, calculated using the Fuller-Schettler-Giddings[9] method, are $Đ_{12} = 2.05$; $Đ_{13} = 1.61$; $Đ_{23} = 3.3 \times 10^{-5}$ $m^2 s^{-1}$; these diffusivities are independent of composition. At the average composition $y_i = \frac{y_{i0} + y_{i\delta}}{2}$, the Fick matrix of diffusivities $[D] = \begin{bmatrix} 1.626 & -0.185 \\ 0.038 & 2.77 \end{bmatrix} \times 10^{-5}$ m^2 s^{-1}. The bootrstrap matrix at the average composition is $[\beta] = \begin{bmatrix} 1.479 & 0.479 \\ 0.0718 & 1.0718 \end{bmatrix}$. The overall effective diffusivity is $[\beta][D] = \begin{bmatrix} 2.426 & 1.05 \\ 0.158 & 2.96 \end{bmatrix} \times 10^{-5}$ m^2 s^{-1}. At steady-state, the transfer fluxes can be estimated as

$$\begin{pmatrix} N_1 \\ N_2 \end{pmatrix} = \frac{101300/(8.314 \times 343.15)}{10^{-3}} \begin{bmatrix} 2.426 & 1.05 \\ 0.158 & 2.96 \end{bmatrix} \times 10^{-5} \begin{pmatrix} 0 - 0.6177 \\ 0 - 0.09264 \end{pmatrix}; \begin{pmatrix} N_1 \\ N_2 \end{pmatrix} = \begin{pmatrix} -0.566 \\ -0.132 \end{pmatrix} \text{ mol } m^{-2} s^{-1}.$$

Both fluxes are directed from liquid to the vapor phase. The ratio of fluxes is $\frac{N_2}{N_1} = 0.233$. This ratio is significantly higher than the ratio of the compositions in the liquid phase $\frac{x_2}{x_1} = 0.15$. The off-diagonal contributions serve to enhance the flux of water because $\frac{0.158}{2.96}\frac{\Delta y_1}{\Delta y_2} = 0.356$ is a significant fractional contribution to the water flux.

Let us now consider diffusional condensation as a strategy for breaking the ethanol/water azeotrope. The bulk vapor is considered to be of composition y_{10} = 0.6177, y_{20} = 0.09264, y_{30} = 0.28971 at temperature T = 343.15 K. This vapor is in contact with a bulk liquid mixture of azeotropic composition at T = 338.15 K. The azeotropic composition at this temperature can be calculated as x_1 = 0.869, x_2 = 0.131, almost identical to the composition at T = 343.15 K. The vapor pressure of ethanol at 338.15 K is 57.5 kPa, and the vapor pressure of water at 338.15 K is 25.03 kPa. The total gas phase pressure p_t =101.3 kPa. The composition of the vapor phase at the gas/liquid interface in equilibrium with the liquid mixture can be calculated from $y_{i0} = \dfrac{\gamma_i x_i P_i^0}{p_t}$. This yields $y_{1\delta} = 0.4989$, $y_{2\delta} = 0.075$, $y_{3\delta} = 0.4261$.

The driving forces are $\Delta y_1 = y_{10} - y_{1\delta} = 0.1188$, and $\Delta y_2 = y_{1o} - y_{2\delta} = 0.01764$. Both driving forces are directed from vapor to the liquid phase. The ratio of driving forces $\dfrac{\Delta y_1}{\Delta y_2} = 6.73$.

The values of the vapor phase M-S diffusivities of the three binary pairs at an average temperature between bulk vapor and interface of 340.65 K, calculated using the Fuller-Schettler-Giddings[9] method, are $Đ_{12} = 2.025$; $Đ_{13} = 1.59$; $Đ_{23} = 3.25\times10^{-5}$ m^{2}s^{-1}; these diffusivities are independent of composition. At the arithmetic average composition $y_i = \dfrac{y_{i0} + y_{i\delta}}{2}$, the Fick matrix of diffusivities $[D] = \begin{bmatrix} 1.61 & -0.2942 \\ 0.06137 & 2.419 \end{bmatrix} \times 10^{-5}$ m^2 s^{-1}. The bootstrap matrix at the average composition is $[\beta] = \begin{bmatrix} 2.56 & 1.56 \\ 0.234 & 1.234 \end{bmatrix}$. The overall effective diffusivity is $[\beta][D] = \begin{bmatrix} 4.226 & 3.02 \\ 0.454 & 2.92 \end{bmatrix} \times 10^{-5}$ m^2 s^{-1}. At steady-state, the transfer fluxes can be estimated as

$$\begin{pmatrix} N_1 \\ N_2 \end{pmatrix} = \frac{101300/(8.314\times340.65)}{10^{-3}} \begin{bmatrix} 4.226 & 3.02 \\ 0.454 & 2.92 \end{bmatrix} \times 10^{-5} \begin{pmatrix} 0.1188 \\ 0.01764 \end{pmatrix}; \begin{pmatrix} N_1 \\ N_2 \end{pmatrix} = \begin{pmatrix} 0.1986 \\ 0..0377 \end{pmatrix}$$ mol m^{-2} s^{-1}. Both fluxes are directed from vapor to the liquid phase. The ratio of fluxes is $\dfrac{N_2}{N_1} = 0.1897$. This ratio is

higher than the ratio of the compositions in the liquid phase $\frac{x_2}{x_1} = 0.15$. The off-diagonal contributions serve to enhance the flux of water because $\frac{0.454}{2.92}\frac{\Delta y_1}{\Delta y_2} = 1.047$ is a significant fractional contribution to the water flux.

5. Transient diffusional evaporation/condensation of ethanol/water/inert vapor

A different method of illustrating the principle of diffusion distillation is to consider transient into a vapor "slab" of half-thickness δ(= 1mm); see schematic in Figure 4. The vapor slab is considered to be of "infinite" length in the vertical direction and the diffusion is limited to the transverse (z) direction.

We first analyze transient diffusional evaporation.

At time t = 0, the bulk vapor phase consists of pure nitrogen: y_{10} = 0.0, y_{20} = 0.0, y_{30} = 1.0.

At time t = 0, either side of the vapor slab is in contact with a binary liquid mixture of constant composition and maintained at 343.15 K. The liquid composition corresponds to the azeotrope: x_1 = 0.869, x_2 = 0.131. The vapor pressure of ethanol at 343.15 K is 71.2 kPa, and the vapor pressure of water at 343.15 K is 31.2 kPa. The total gas phase pressure p_t =101.3 kPa. The composition of the vapor phase at the gas/liquid interface in equilibrium with the liquid mixture can be calculated from $y_{i0} = \frac{\gamma_i x_i P_i^0}{p_t}$. This yields $y_{1\delta}$ = 0.6177, $y_{2\delta}$ = 0.09264, $y_{3\delta}$ = 0.28971.

For a binary vapor mixture, the fractional *departure* from equilibrium is given by the matrix equation

$$\bar{y}(t) - y_{z=\delta} = Q(y_0 - y_{z=\delta}); \quad Q \equiv \sum_{m=0}^{\infty} \frac{8}{(2m+1)^2 \pi^2} \exp\left[-(2m+1)^2 \pi^2 \frac{Dt}{4\delta^2}\right] \tag{27}$$

This expression can be generalized for ternary vapor mixtures by using two-dimensional matrix notation by replacing the binary mixture diffusivity D by $[\beta][D]$; the justification for this procedure is provided in earlier works. [3, 6]

The expression for fractional *departure* from equilibrium for ternary vapor mixtures (inert species 3) is

$$\left(\overline{y}(t)-y_{z=\delta}\right)=[Q]\left(y_0-y_{z=\delta}\right);\quad [Q]\equiv\sum_{m=0}^{\infty}\frac{8}{(2m+1)^2\pi^2}\exp\left[-(2m+1)^2\pi^2\frac{[\beta][D]t}{4\delta^2}\right] \tag{28}$$

The Sylvester theorem, detailed in Appendix A of Taylor and Krishna,[3] is required for explicit calculation of $[Q]$. For the case of distinct eigenvalues, λ_1 and λ_2 of the the 2-dimensional square matrix $[\beta][D]$, the Sylvester theorem yields

$$[Q]=\frac{f(\lambda_1)[[\beta][D]-\lambda_2[I]]}{(\lambda_1-\lambda_2)}+\frac{f(\lambda_2)[[\beta][D]-\lambda_1[I]]}{(\lambda_2-\lambda_1)} \tag{29}$$

In equation (29), $[I]$ is the identity matrix with elements δ_{ik}. The functions $f(\lambda_i)$ are obtained by substituting the eigenvalues λ_1 and λ_2 in place of the binary diffusivity in equation (27):

$$f(\lambda_i)=\sum_{m=0}^{\infty}\frac{8}{(2m+1)^2\pi^2}\exp\left[-(2m+1)^2\pi^2\frac{\lambda_i t}{4\delta^2}\right] \tag{30}$$

The calculations can be easily implemented in MathCad 15.[10] A printout of the MathCad file is appended along with this Supplementary material.

In Figure 5a, the spatial-averaged mole fractions $\left(\overline{y}(t)\right)$of ethanol (1) and water (2) are plotted as a function of time, *t*. The ratio of the mole fraction of water (2) to that of ethanol (1) in the vapor phase as a function of time, *t* is plotted in Figure 5b; this ratio equilibrates to the value of $\frac{y_2}{y_1}=\frac{x_2}{x_1}=0.15$, as is expected. During the initial transience, however, $\frac{y_2}{y_1}>\frac{x_2}{x_1}=0.15$, i.e. the vapor phase is richer in water than the azeotropic composition. Short contact times result in more effective separations. Figure 5b compares the transient values of $\frac{y_2}{y_1}$ for nitrogen, argon, and helium. We note that best separations are obtained by choosing argon as the inert gas.

Figure 5c plots the equilibration trajectories in ternary composition space. Using the Maxwell-Stefan diffusion equations, the trajectories follow curvilinear paths. The azeotrope is broken precisely because the equilibration trajectory is not linear in composition space.

We first analyze transient diffusional condensation.

At time $t = 0$, the composition of the vapor slab is $y_{10} = 0.6177$, $y_{20} = 0.09264$, $y_{30} = 0.28971$ at 343.15 K. The two sides of the vapor slab are in contact with a binary liquid mixture of constant composition and maintained at 338.15 K. The liquid composition corresponds to the azeotrope: $x_1 = 0.869$, $x_2 = 0.131$, almost identical to the composition at $T = 343.15$ K. The vapor pressure of ethanol at 338.15 K is 57.5 kPa, and the vapor pressure of water at 338.15 K is 25.03 kPa. The total gas phase pressure p_t =101.3 kPa. The composition of the vapor phase at the gas/liquid interface in equilibrium with the liquid mixture can be calculated from $y_{i0} = \dfrac{\gamma_i x_i P_i^0}{p_t}$. This yields $y_{1\delta} = 0.4989$, $y_{2\delta} = 0.075$, $y_{3\delta} = 0.4261$.

The calculations can be easily implemented in MathCad 15.[10]

In Figure 6a, the spatial-averaged mole fractions $\left(\overline{y}(t)\right)$of ethanol (1) and water (2) are plotted as a function of time, t. The ratio of the mole fraction of water (2) to that of ethanol (1) in the vapor phase as a function of time, t is plotted in Figure 6b; this ratio equilibrates to the value of $\dfrac{y_2}{y_1} = \dfrac{x_2}{x_1} = 0.15$, as is expected. During the initial transience, however, $\dfrac{y_2}{y_1} < \dfrac{x_2}{x_1} = 0.15$, i.e. the vapor phase is poorer in water than the azeotropic composition. Shorter contact times result in more effective separations. Figure 5b compares the transient values of $\dfrac{y_2}{y_1}$ for nitrogen, argon, and helium. We note that best separations are obtained by choosing argon as the inert gas.

Figure 6c plots the equilibration trajectories in ternary composition space. Using the Maxwell-Stefan diffusion equations, the trajectories follow curvilinear paths. The azeotrope is broken precisely because the equilibration trajectory is not linear in composition space.

The important message that emerges from the transient equilibration simulations is that the contact time between the vapor and liquid phases is crucial to the separation of azeotropic mixtures.

6. Distillation of water/ethanol/methanol/acetone mixtures

Experimental data for Murhpree efficiencies for quaternary water(1)/ethanol(2)/methanol(3)/acetone(4) mixtures were determined by Springer et al.[11] The experiments were carried out in a 12-stage bubble capd distillation column wherein all the experiments were conducted under total-reflux conditions at 101.3 kPa. Table 2 provides the data on the liquid compositions leaving each stage for Run Q6. The experimental composition trajectories in the column are indicated by the blue circles in Figure 7. The data are plotted in ternary composition space by combining the mole fractions of methanol and acetone in the left bottom vertex.

Two distillation boundaries are shown in Figure 7: the "acetone" boundary is the same as for the water/ethanol/acetone mixture; the "methanol" boundary is the same as for the water/ethanol/methanol mixture. The experimental data shows that both the "acetone" and "methanol" boundaries are crossed in Run Q6. Also shown as insets are the Murphree component efficiencies and component driving forces. The component Murphree efficiency of methanol is negative on stage 3, and slightly exceeds unity on stage 4. This implies that uphill diffusion of methanol manifests on stage 4. The reason is to found in the fact that the driving force of methanol is practically zero on these two stages; the direction of transport of methanol is dictated by the transfer of the three partner species in the mixture: water, ethanol, and acetone. The boundary crossing is primarily due to the factor that the Murphree efficiency of water is higher than that of ethanol, i.e. $E_1 > E_2$.

7. Transient equilibration inside vapor bubble rising through a liquid on a distillation tray

Let us try to verify the phenomenon of uphill diffusion of methanol by a simple model. Let us consider the dispersion to consist of uniform and rigid vapor bubbles of diameter, d_{bubble}. The transient equilibration process within a rigid spherical bubble is described by Geddes model that was originally

developed for describing binary diffusion inside vapor bubbles on distillation trays.[12] For ternary mixtures, the Geddes model can be written in 3-dimensional matrix equation[3, 13]

$$\left(y_L - y_{eq}\right) = [Q]\left(y_E - y_{eq}\right); \quad [Q] \equiv \frac{6}{\pi^2}\sum_{m=1}^{\infty}\frac{1}{m^2}\exp\left[-m^2\pi^2\frac{4[D]t}{d_{bubble}^2}\right] \tag{31}$$

In Equation (31), $\left(y_E\right)$ denotes the vapor composition entering the tray, $\left(y_{eq}\right)$ denotes the vapor composition in equilibrium with the liquid leaving the tray, $\left(x_L\right)$, and $\left(y_L\right)$ denotes the vapor composition in leaving the tray; see schematic in Figure 8. For a tray operating at total reflux, the compositions of the vapor entering any stage, equals the compositions of the liquid leaving the stage, i.e. $\left(y_E\right) = \left(x_L\right)$. Table 3 provides the NRTL parameters used in the calculation of the vapor/liquid phase equilibrium.

The elements of the Fick diffusivity matrix [*D*] can be explicitly calculated from equation (13). The M-S vapor phase diffusivity of the binary pairs, estimated from Fuller-Schettler-Giddings[9] method are provided in Table 4.

The Sylvester theorem, detailed in Appendix A of Taylor and Krishna,[3] is required for explicit calculation of $[Q]$. For the case of three distinct eigenvalues, λ_1, λ_2, and λ_3 of the 3-dimensional square matrix $[D]$, the Sylvester theorem yields

$$[Q] = \frac{f(\lambda_1)[[D]-\lambda_2[I]][[D]-\lambda_3[I]]}{(\lambda_1-\lambda_2)(\lambda_1-\lambda_3)} + \frac{f(\lambda_2)[[D]-\lambda_1[I]][[D]-\lambda_3[I]]}{(\lambda_2-\lambda_1)(\lambda_2-\lambda_3)} + \frac{f(\lambda_3)[[D]-\lambda_1[I]][[D]-\lambda_2[I]]}{(\lambda_3-\lambda_1)(\lambda_3-\lambda_2)} \tag{32}$$

In equation (32), $[I]$ is the identity matrix with elements δ_{ik}. The functions $f(\lambda_i)$ are calculated from

$$f(\lambda_i) = \frac{6}{\pi^2}\sum_{m=1}^{\infty}\frac{1}{m^2}\exp\left[-m^2\pi^2\frac{4\lambda_i t}{d_{bubble}^2}\right] \tag{33}$$

For vapor bubbles rising on a sieve or bubble-cap tray, the effective contact time of the dispersed phase bubbles with the surrounding continuous phase is $t = h_f / V_{bubble}$, where h_f is the froth dispersion height, and V_{bubble} is the bubble rise velocity.

The fractional approaches to equilibrium for contact time *t*, also termed as the Murphree efficiencies,[14-16] are calculated from

$$E_i = \frac{y_{iE} - y_{iL}}{y_{iE} - y_{i,eq}}; \quad i = 1,2,..n \tag{34}$$

Figure 9 presents the Geddes model calculations for the Murhpree point efficiencies on Stages 2, 3, 4, 5, 6 and 7. The inlet compositions on the stages are as specified in Table 2. The *x*-axis is the contact time. The bubble diameter used in the simulations correspond to the value determined experimentally to be 5 mm. In the experimental set-up the vapor/liquid contact time on the tray is 0.046 s.

The simulations show the hierarchy of component efficiencies $E_1 > E_2 \approx E_4$; this is in good agreement with the experimental data in Figure 7.

For stage 4, we note that the efficiency of methanol exceeds unity, indicating uphill diffusion. This is in accord with the data of Springer et al.[11] in Figure 7.

Figure 10 shows the equilibration trajectory for water(1)/ethanol(2)/methanol(3)/acetone(4) mixtures for entering vapor compositions $y_{1E} = 0.11; y_{1E} = 0.79; y_{1E} = 0.08; y_{1E} = 0.02$. We note that the equilibration trajectory has crossed the water/ethanol/acetone "distillation boundary". These calculations provide a rationalization of the experimental observation of boundary crossing in Figure 7.

8. Notation

c_t	total molar concentration of mixture, mol m^{-3}
d_{bubble}	bubble diameter, m
$[B]$	inverse diffusivity matrix, m^{-2} s^{1}
$Đ_{ij}$	M-S binary pair diffusivity, m^2 s^{-1}
$[D]$	Fick diffusivity matrix, m^2 s^{-1}
E_i	Component Murphree efficiency, dimensionless
h_f	froth height on distillation tray, m
$[I]$	Identity matrix, dimensionless
J_i	molar diffusion flux of species *i* with respect to u, mol m^{-2} s^{-1}
V_i	molar diffusion flux of species *i* in laboratory fixed reference frame, mol m^{-2} s^{-1}
p_i	partial pressure, Pa
p_t	total pressure, Pa
P_i^0	vapor pressure, Pa
$[Q]$	matrix quantifying fractional departure from equilibrium, dimensionless
R	gas constant, 8.314 J mol^{-1} K^{-1}
t	time, s
T	absolute temperature, K
x_i	mole fraction of component *i* in liquid phase, dimensionless
y_i	mole fraction of component *i* in vapor phase, dimensionless
u	molar average mixture velocity, m s^{-1}
V_{bubble}	bubble rise velocity, m s^{-1}
z	direction coordinate, m

Greek letters

δ	film thickness, m
δ_{ij}	Kronecker delta, dimensionless
γ_i	activity coefficient of component *i*, dimensionless

Subscript

0	Referring to starting compositions, $t = 0$
bubble	Referring to bubble
eq	Referring to final equilibrated compositions, $t \to \infty$
E	Referring to vapor compositions entering tray
i	Component number
j	Component number
L	referring to compositions leaving tray
O	referring to overall parameter

Table 1. NRTL parameters for ethanol(1)/water (2) mixture. These parameters are from the DECHEMA Dortmund data bank, and are used along with $G_{ij} = \exp\left(-\alpha_{ij}\tau_{ij}\right)$.

Component 1	Component 2	τ_{12}	τ_{21}	α_{12}
ethanol(1)	water (2)	$\tau_{12} = -\frac{29.169}{T}$	$\tau_{21} = \frac{624.9174}{T}$	0.2937

Table 2. Compositions of the liquid leaving each stage for Run Q6 of Springer. At total reflux, the compositions leaving each stage equals the vapor entering each stage. These compositions were determined by a non-equilibrium stage model that matched the column composition profiles that were determined in the experiments.

Stage number	x_{1E}	x_{2E}	x_{3E}	x_{4E}
1	0.0109	0.152	0.1839	0.6532
2	0.0205	0.2865	0.1956	0.4974
3	0.0307	0.3658	0.1986	0.4049
4	0.0446	0.4576	0.197	0.3008
5	0.0614	0.5527	0.1868	0.199
6	0.0787	0.6374	0.167	0.1169
7	0.094	0.7026	0.1412	0.0622
8	0.1064	0.748	0.1147	0.031
9	0.1163	0.778	0.0908	0.0149
10	0.1245	0.7977	0.0709	0.006964
11	0.1316	0.8103	0.0549	0.003223
12	0.1381	0.818	0.0424	0.00148

Table 3. The NRTL parameters for the quaternary mixture water (1) – ethanol (2) – methanol (3) – acetone (4) at 101.3 kPa (Gmehling & Onken, 1977).

These parameters are used along with $G_{ij} = \exp(-\alpha_{ij}\,\tau_{ij})$ and $\tau_{ij} = B_{ij}/T$

Quaternary system (homogeneous)				
Component *i*	Component *j*	B_{ij} / [K]	B_{ji} / [K]	α_{ij} / [-]
Water	Ethanol	624.9174	-29.169	0.2937
Water	Methanol	594.6299	-182.6052	0.297
Water	Acetone	602.6252	330.4768	0.5103
Ethanol	Methanol	73.413	-79.1718	0.3029
Ethanol	Acetone	188.8983	22.83319	0.3006
Methanol	Acetone	97.78178	107.83	0.3008

Table 4. M-S vapor phase diffusivities for the binary pairs in the quaternary Water (1) – Ethanol (2) – Methanol (3) – Acetone (4) system. The values are calculated using the FSG correlation at the temperature 340 K, the average temperature in Run Q6 in the Springer experiments.

Parameter	units	i-j pair					
		1-2 pair	1-3 pair	1-4 pair	2-3 pair	2-4 pair	3-4 pair
$Đ_{ij}$	10^{-5} m^2 s^{-1}	2.1	2.72	1.82	1.36	0.908	1.18

9. References

(1) Maxwell, J. C. On the dynamical theory of gases. *Phil. Trans. Roy. Soc.* **1866**, *157*, 49-88.

(2) Stefan, J. Über das Gleichgewicht und die Bewegung insbesondere die Diffusion von Gasgemengen. *Sitzber. Akad. Wiss. Wien.* **1871**, *63*, 63-124.

(3) Taylor, R.; Krishna, R. *Multicomponent mass transfer*; John Wiley: New York, 1993.

(4) Krishna, R. Uphill Diffusion in Multicomponent Mixtures. *Chem. Soc. Rev.* **2015**, *44*, 2812-2836.

(5) Krishna, R.; Standart, G. L. A multicomponent film model incorporating a general matrix method of solution to the Maxwell-Stefan equations. *A.I.Ch.E.J.* **1976**, *22*, 383-389.

(6) Krishna, R. An alternative linearized theory of multicomponent mass transfer. *Chem. Eng. Sci.* **1981**, *36*, 219-222.

(7) Fullarton, D.; Schlünder, E. U. Diffusion Distillation - A New Separation .Process for Azeotropic Mixtures - Part I: Selectivity and Transfer Efficiency. *Chem. Eng. Process.* **1986**, *20*, 255-263.

(8) Singh, N.; Prasad, R. Experimental studies on the effect of inert gases on diffusion distillation of ethanol–water mixtures. *J. Chem. Technol. Biotechnol.* **2011**, *86*, 1495-1500.

(9) Fuller, E. N.; Schettler, P. D.; Giddings, J. C. A New Method for Prediction of Binary Gas-phase Diffusion Coefficients. *Ind. Eng. Chem.* **1966**, *58*, 19-27.

(10) PTC MathCad 15.0. http://www.ptc.com/, PTC Corporate Headquarters, Needham, 3 November 2015.

(11) Springer, P. A. M.; van der Molen, S.; Baur, R.; Krishna, R. Experimental verification of the necessity to use the Maxwell-Stefan formulation in describing trajectories during azeotropic distillation. *Chem. Eng. Res. Des.* **2002**, *80*, 654-666.

(12) Geddes, R. L. Local efficiencies of bubble-plate fractionators. *Trans. Am. Inst. Chem. Engrs.* **1946**, *42*, 79-105.

(13) Krishna, R. Model for prediction of point efficiencies for multicomponent distillation. **1985**, *63*, 312-322.

(14) Treybal, R. E. *Mass-Transfer Operations*; 3rd Edition, McGraw-Hill: New York, 1980.

(15) Robbins, L. A.; Cusack, R. W. *Chaper 15, Liquid-Liquid Extraction Operations and Equipment*. Perry's Chemical Engineers' Handbook; 7th Edition, Edited by R.H. Perry and D.W. Green, McGraw-Hill: New York, 1999.

(16) Seader, J. D.; Henley, E. J.; Roper, D. K. *Separation Process Principles*; 3rd Edition, John Wiley: New York, 2011.

10. Caption for Figures

Figure 1. A force balance on a control volume containing an ideal gas mixture.

Figure 2. The force acting on each of the species in the diffusing mixture is balanced by friction between the species 1 and 2.

Figure 3. Schematic for liquid/vapor transfer for ethanol (1)/ water (2)/nitrogen (3) at steady state across a film of thickness δ.

Figure 4. Schematic for transient diffusion of ethanol/water into slab of half-thickness δ.

Figure 5. Transient equilibration in the vapor phase for ethanol (1)/ water (2)/inert (3) caused by diffusional evaporation. (a) The mole fractions of ethanol (1) and water (2) plotted as a function of time, *t*.The total pressure is 101.3 kPa, and the temperature is 340.65 K. (b) Comparisons of the ratios of the mole fraction of water (2) to that of ethanol (1) in the vapor phase as a function of time, *t* using nitrogen, argon, and helium as inert gas. (c) Comparison of diffusion equilibration trajectories in composition space.

Figure 6. Transient equilibration in the vapor phase for ethanol (1)/ water (2)/inert (3) caused by diffusional evaporation. (a) The mole fractions of ethanol (1) and water (2) plotted as a function of time, *t*.The total pressure is 101.3 kPa, and the temperature is 340.65 K. (b) Comparisons of the ratios of

the mole fraction of water (2) to that of ethanol (1) in the vapor phase as a function of time, *t* using nitrogen, argon, and helium as inert gas. (c) Comparison of diffusion equilibration trajectories in composition space.

Figure 7. Experimental data (blue circles) of Springer et al.[11] for Run Q6 with quaternary water(1)/ethanol(2)/methanol(3)/acetone(4) mixtures. Also shown as insets are the Murphree component efficiencies and component driving forces.

Figure 8. Vapor-liquid contacting on distillation tray.

Figure 9. Geddes model calculations for the Murhpree point efficiencies on Stages 2, 3, 4, 5, 6, and 7. The liquid compositions leaving each stage (= vapor composition entering that stage) are as specified in Table 2.

Figure 10. Equilibration trajectory for water(1)/ethanol(2)/methanol(3)/acetone(4) mixtures calculated with the Geddes model.[12]

Fig. S1

Force balance

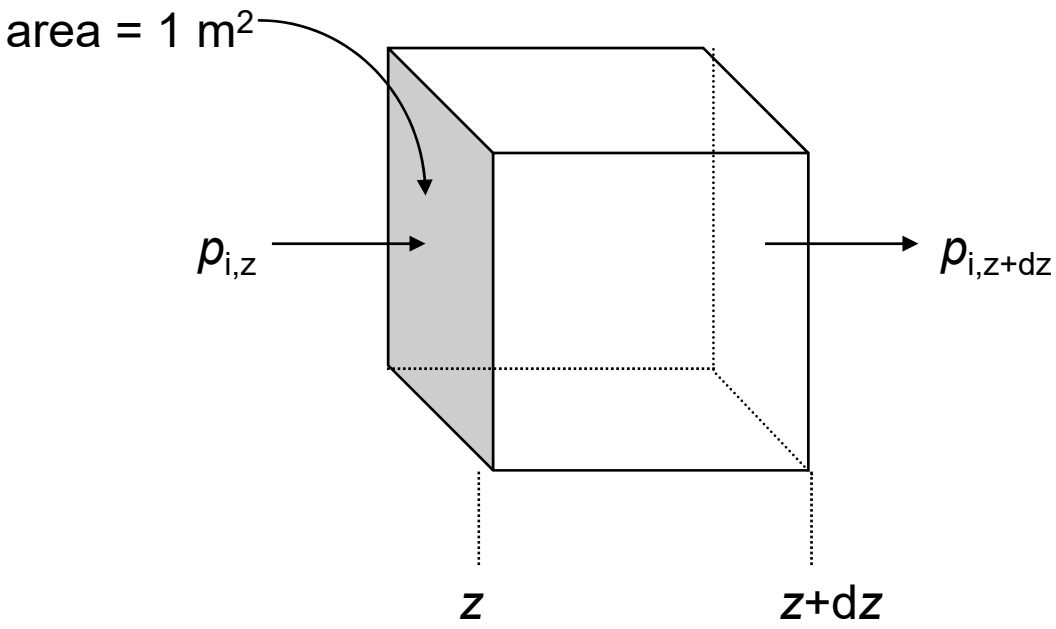

Fig. S2

Force is balanced by friction

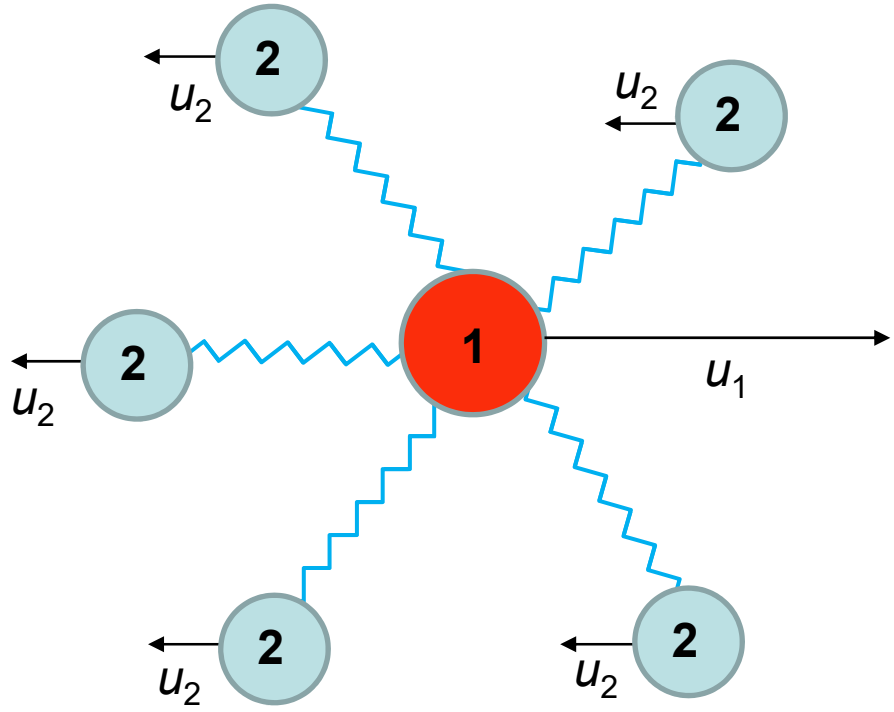

Force acting per mole of species 1

=

Friction between 1 and 2

Fig. S3

Steady-state diffusion into vapor slab

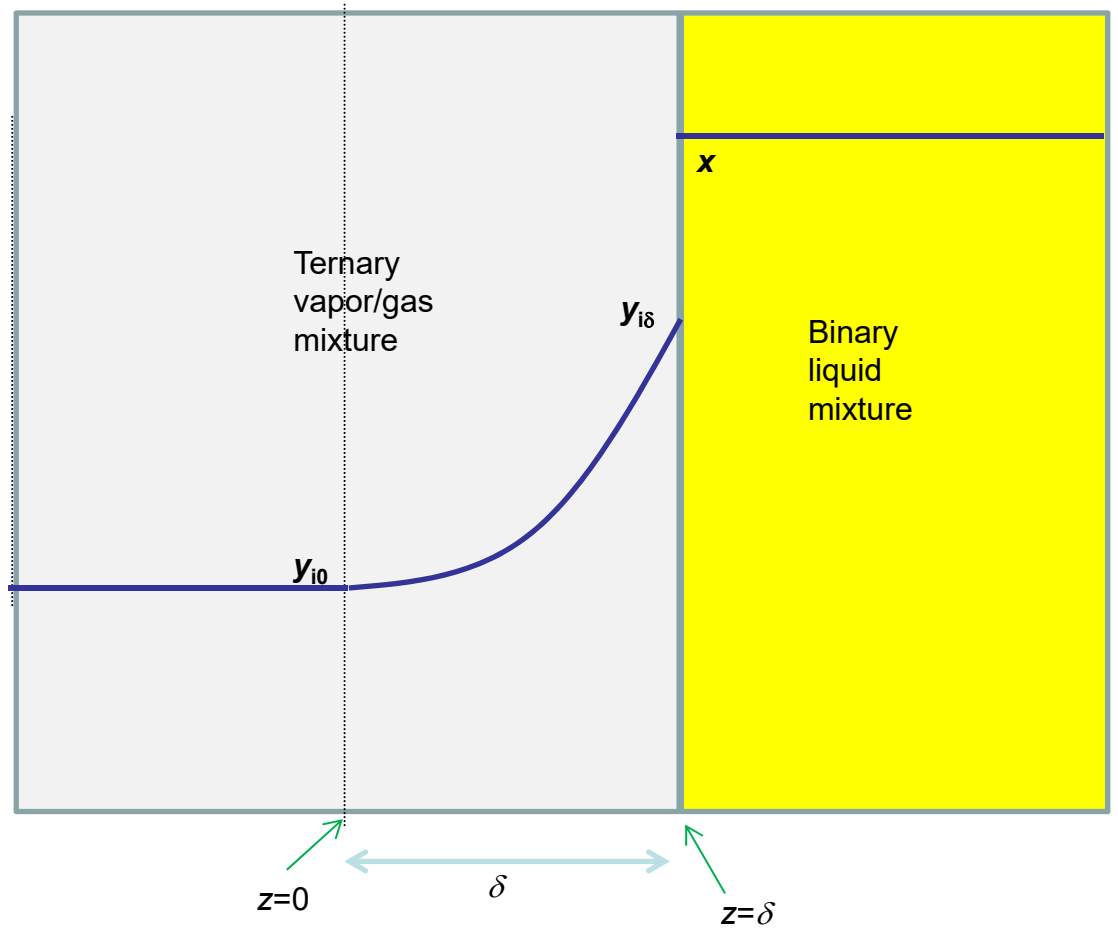

Fig. S4

Transient diffusion into vapor slab

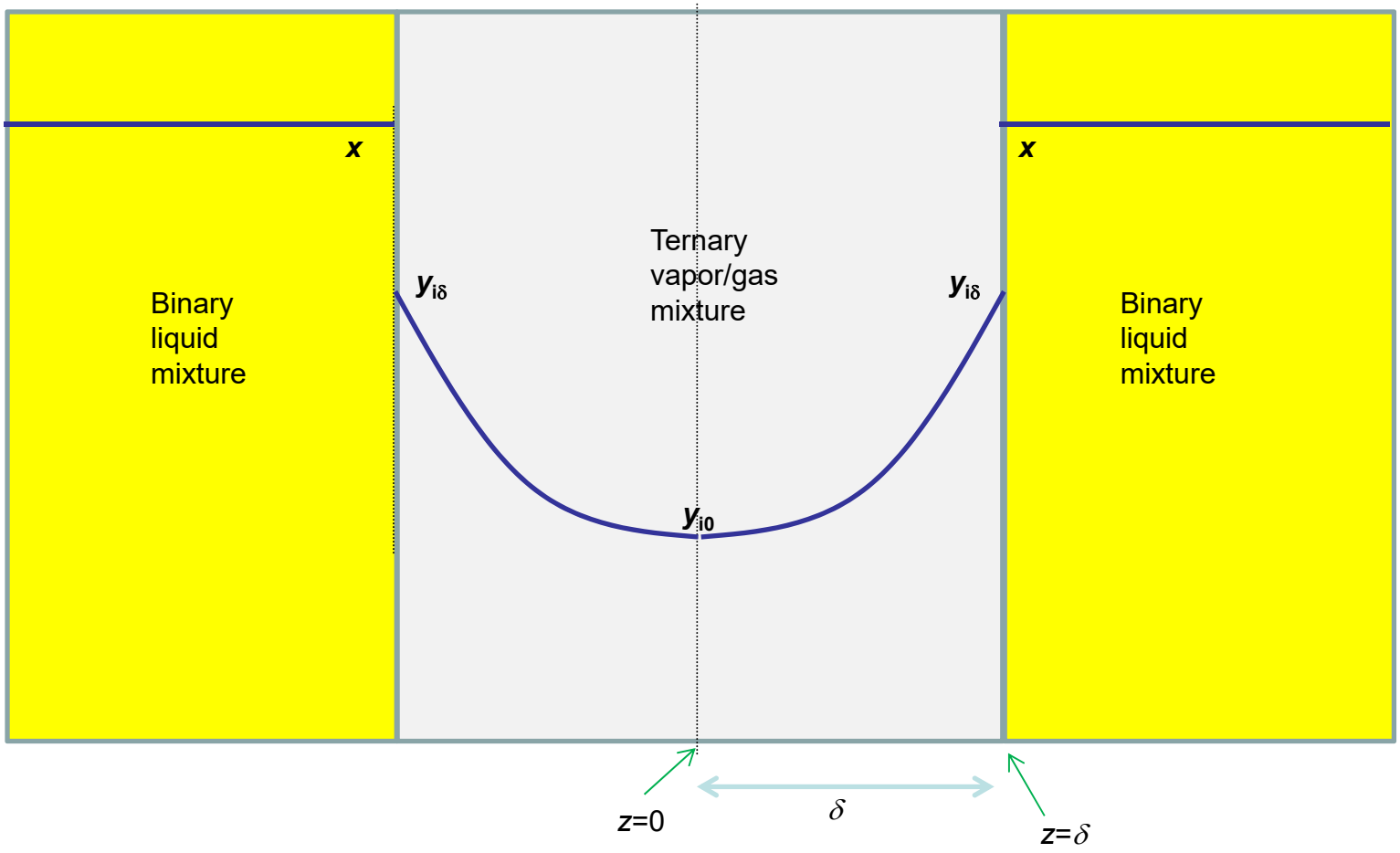

Ethanol/water/inert: diffusional evaporation

Fig. S5

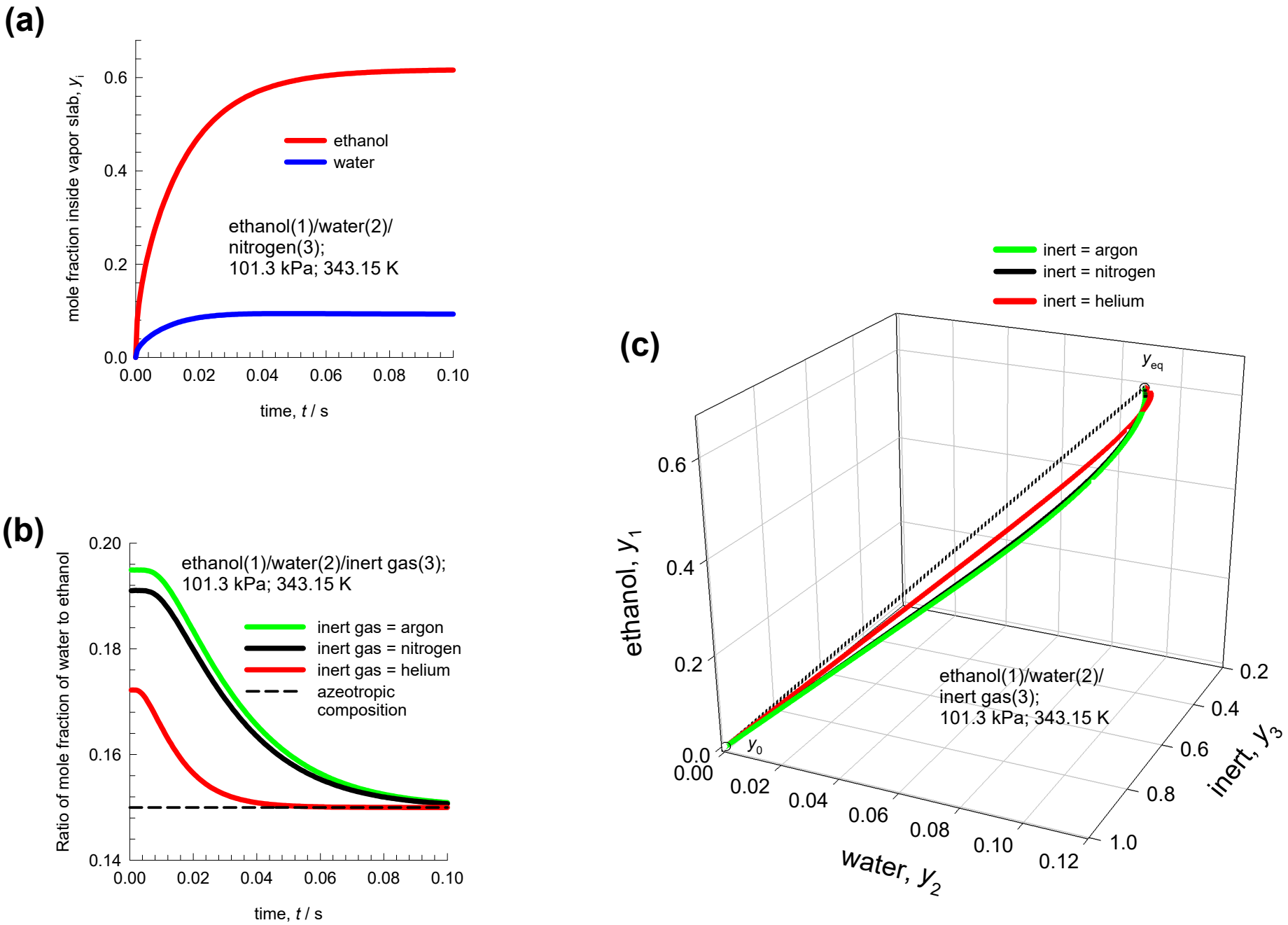

Ethanol/water/inert: diffusional condensation

Fig. S6

(a)

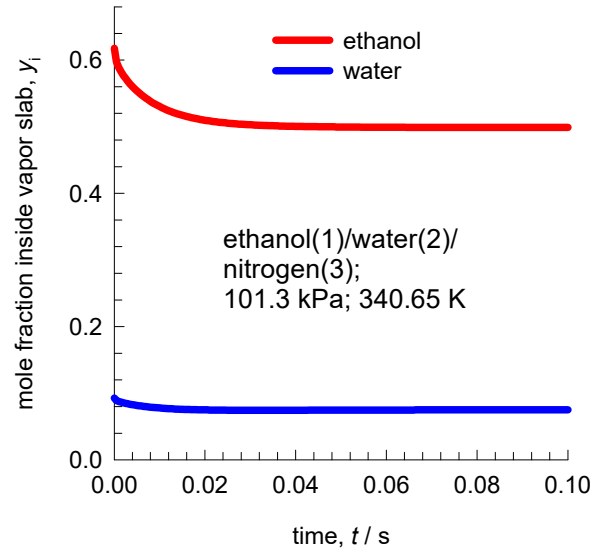

(b)

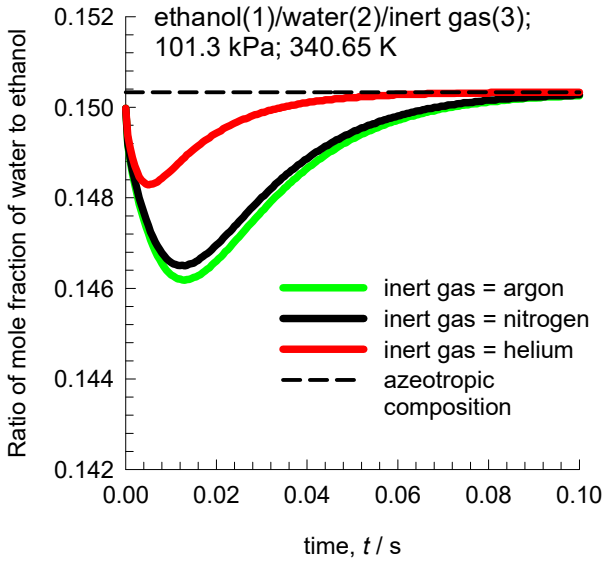

(c)

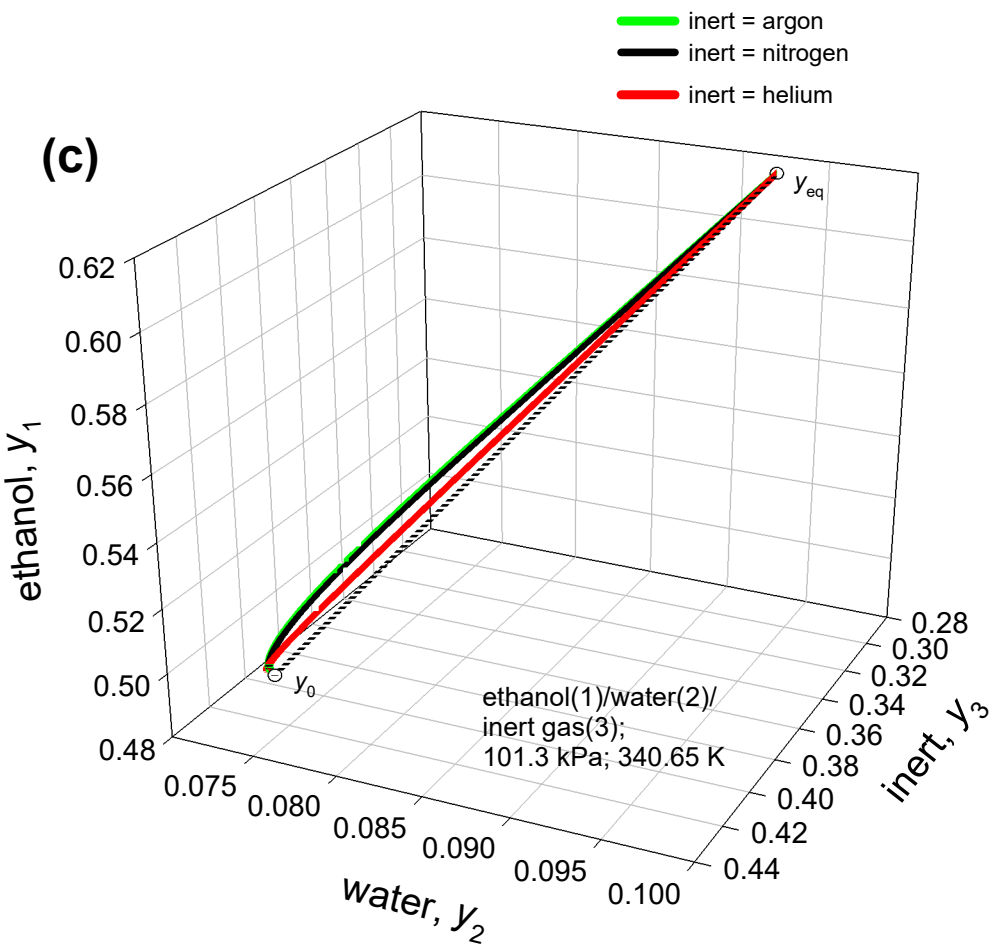

Water/Ethanol/Acetone/Methanol Distillation

Fig. S7

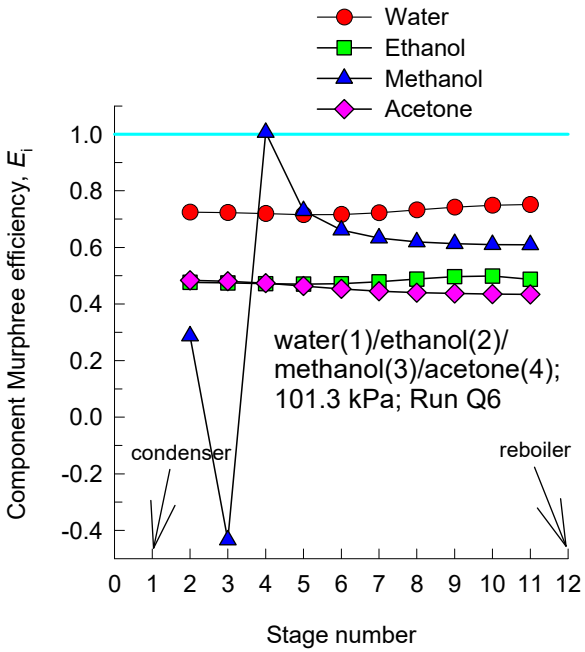

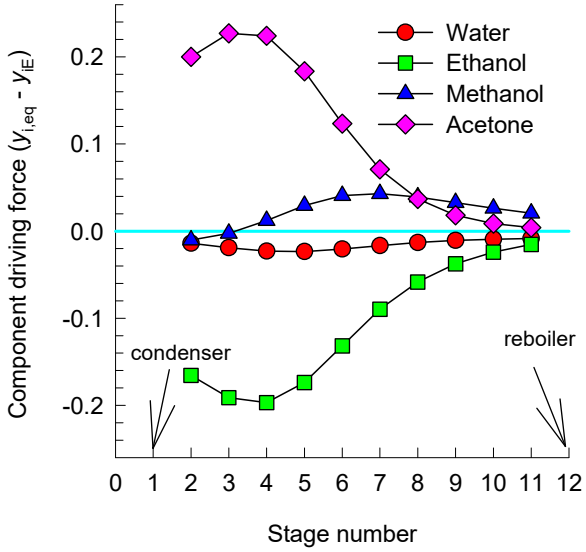

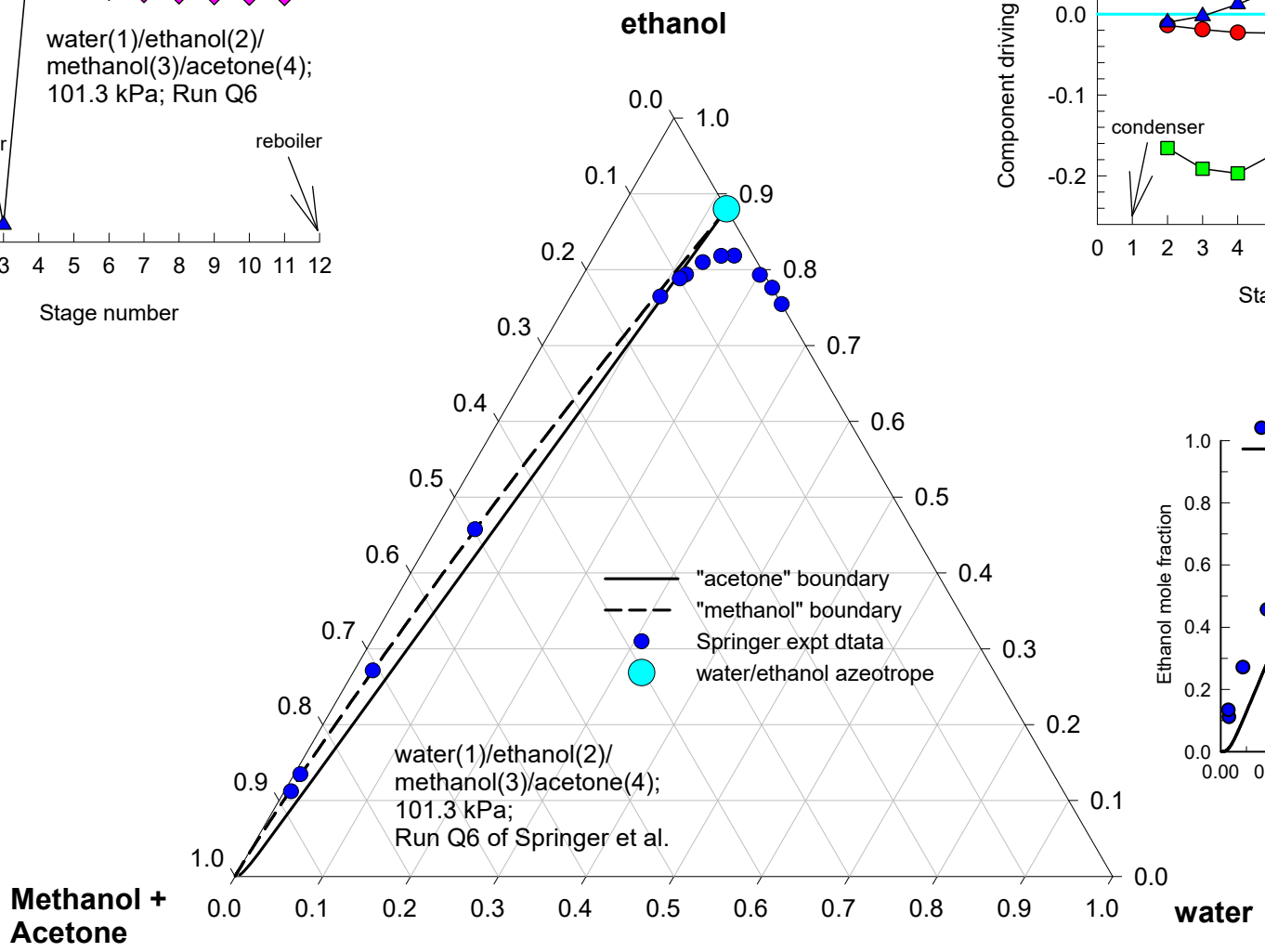

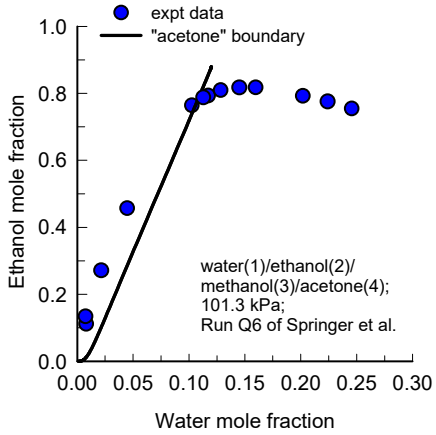

Fig. S8

Vapor/liquid contacting on distillation tray

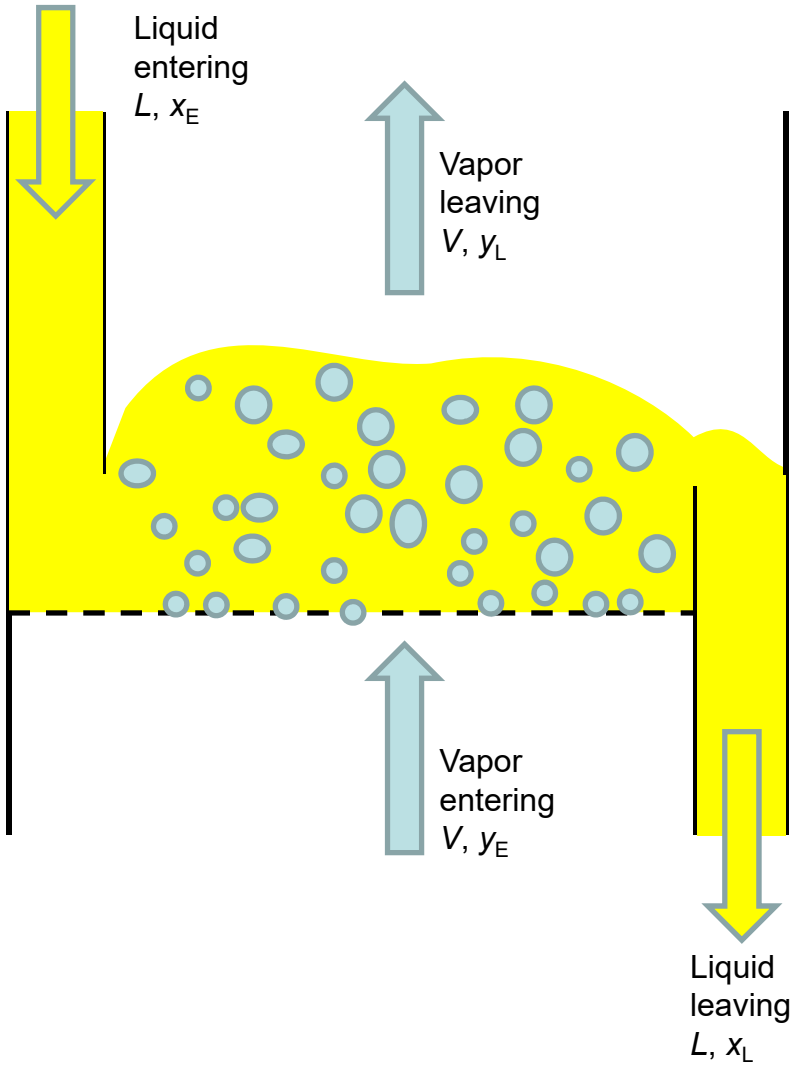

Fig. S9

Murphree Point Efficiencies: Geddes model

(a) Stage 2

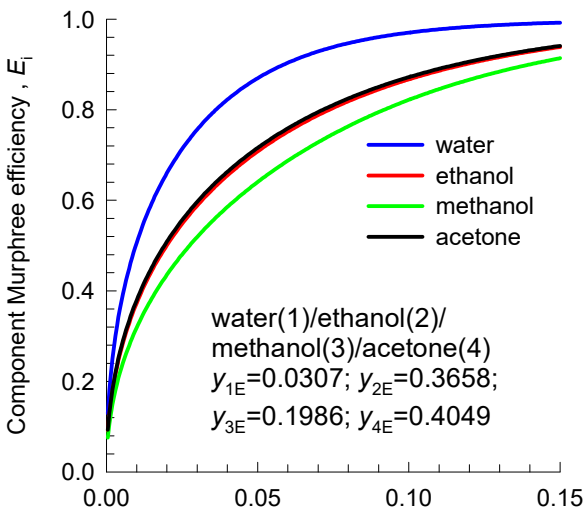

(b) Stage 3

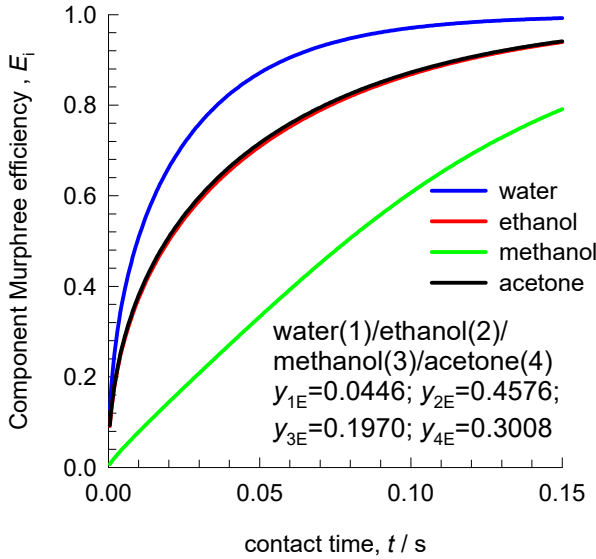

(c) Stage 4

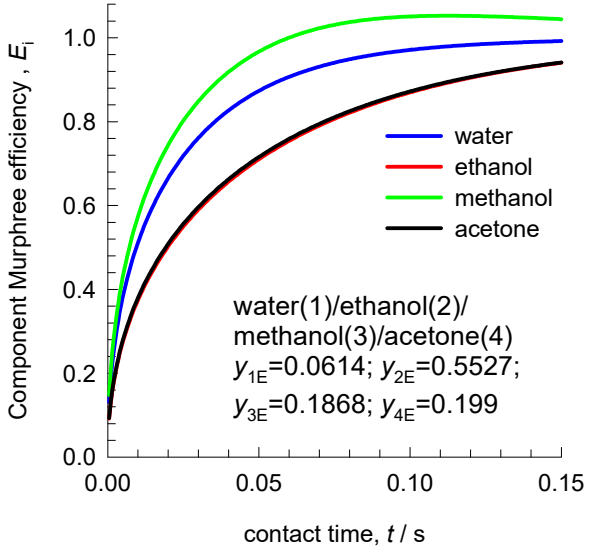

(d) Stage 5

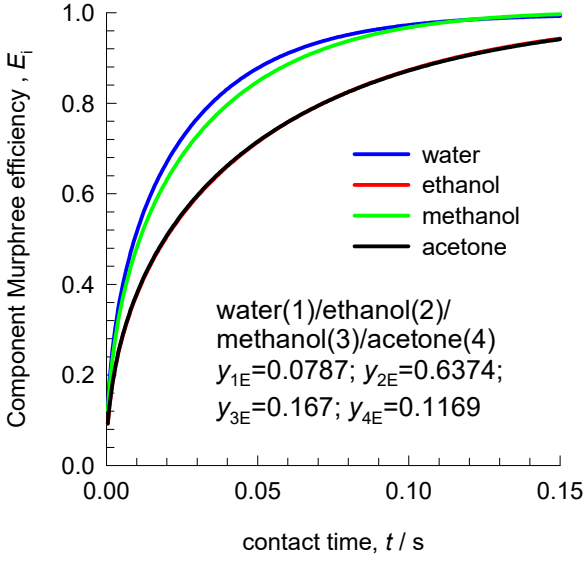

(e) Stage 6

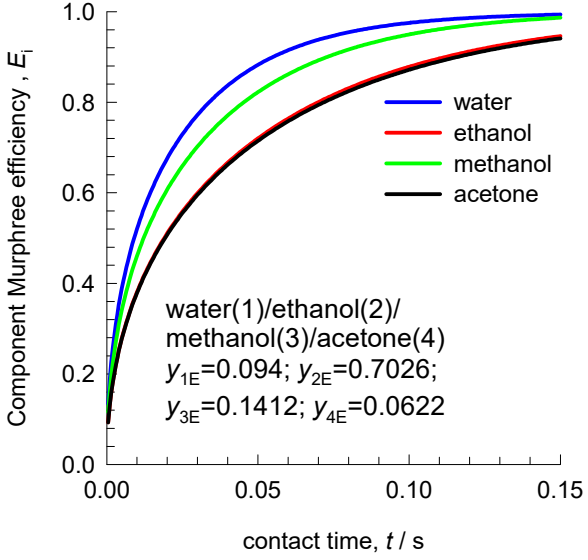

(f) Stage 7

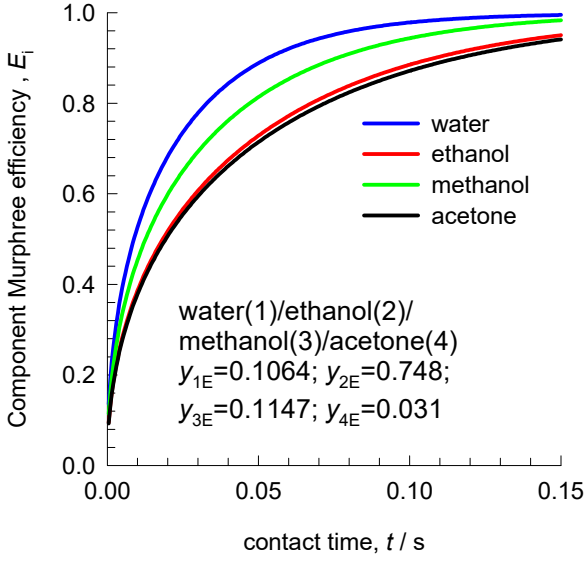

Fig. S10

Boundary crossing with Geddes model